CHEMISTRY OF MATERIALS

pubs.acs.org/cm

Article

Rapid Photoligation of Gold Nanocolloids with Lipoic Acid-Based Ligands

Zhicheng Jin, Yuya Sugiyama, Chengqi Zhang, Goutam Palui, Yan Xin, Liang Du, Sisi Wang, Narjes Dridi, and Hedi Mattoussi*

Cite This: *Chem. Mater.* 2020, 32, 7469−7483

Read Online

ACCESS | Metrics & More | Article Recommendations | Supporting Information

ABSTRACT: An effective and easy to implement ligand exchange strategy is paramount to the design of stable and multifunctional gold and other inorganic nanocolloids. This is also crucial for their use in biology and medicine. In this contribution, we demonstrate that photomediated ligand substitution of gold nanocrystals with a series of lipoic acid-modified ligands yields several advantages, including rapid phase transfer and great long-term colloidal stability. This strategy combines photochemical reduction of the dithiolane group with energetically favorable *in situ* ligand chemisorption, yielding rapid modification of the surfaces. It requires substantially smaller amounts of excess ligands compared to conventional incubation starting with the oxidized form of the ligands. Complete substitution of the ligands is confirmed by using ^{1}H NMR and FT-IR spectroscopy. The colloidal properties of the resulting materials have been tested by using a combination of long-term stability in ion-rich media, sodium cyanide digestion, and dithiothreitol competition tests. They show that photoligation preserves the structure and photophysical properties of the various colloids. Mechanistic arguments have been discussed to explain the effectiveness of this ligation strategy. These findings prove the practical benefits of this approach for designing biocompatible gold colloids and bode well for using such materials in a variety of biological assays and photothermal therapy.

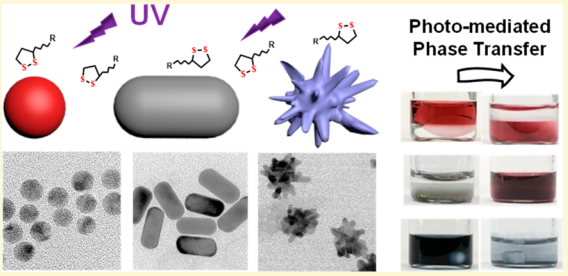

INTRODUCTION

In recent years, gold nanocolloids such as nanoparticles (AuNPs), nanorods (AuNRs), and nanostars (AuNSs) have generated tremendous interest and much activity in areas ranging from electronic devices to biomedical research.[1−8] These materials exhibit several unique properties ranging from unique size- and shape-dependent optical properties to strong near-field interactions with proximal dye emitters and Raman-active molecules, which have found applications in sensor design and biomedicine.[3,8−13] For example, spherical AuNPs (with a diameter of 4−50 nm) exhibit a surface plasmon resonance (SPR) band at ∼520 nm, and they have been widely utilized in colorimetric and energy-transfer-based assays.[13−15] In comparison, anisotropic AuNRs and AuNSs show an additional longitudinal strong SPR peak in the near-infrared (NIR) region of the optical spectrum, with substantially larger molar absorption coefficients than those measured for the smaller spherical AuNPs.[4,16−18] The pronounced longitudinal absorption, combined with the deep penetration of NIR irradiation into tissues, makes these materials ideal candidates for use in photothermal therapy to treat cancer.[6,11,19] These bioapplications require optimized interfacing between the gold nanocolloids and biomolecules to enhance their performance in biological settings. Broadly, surface functionalization strategies for such materials can be grouped into encapsulation and ligand exchange.[6,20−28] Encapsulation within amphiphilic polymers or micelles is easy to implement and does not require removal of the native cap, which potentially preserves the photophysical properties of the original materials; however, it tends to yield colloids with large coatings and limited colloidal stability.[29−31] Ligand exchange, in comparison, involves substitution of the native cap with bifunctional ligands that contain hydrophilic blocks to provide water solubility along with metal-chelating groups for promoting coordination onto the nanomaterial surfaces. It tends to yield strong binding and offer more control over the coating structure. Among the anchoring groups explored, soft Lewis bases, including monothiol and bidentate thiols and phosphines, are known to strongly coordinate onto gold surfaces (rich in soft Lewis acid Au).[7,32,33] A variety of thiol-modified molecules have been designed and tested for coating Au surfaces with great success.[27,34−38]

Conventional cap exchange of Au colloids with lipoic acid-appended compounds (LA-R ligands) has attracted much attention due to their bidentate nature, but when used in their

Received: June 14, 2020
Revised: July 28, 2020
Published: July 29, 2020

https://dx.doi.org/10.1021/acs.chemmater.0c02482
Chem. Mater. 2020, 32, 7469−7483

oxidized form, they require a long reaction/incubation time, that is, several hours to a few days.[28,35,38−42] The procedure also consumes large amounts of ligands, since the ligand substitution relies on mass action kinetics. Our group and others have shown that overnight incubation with a multi-LA polymer under mild heating conditions (at ∼50 °C) promotes cap exchange with AuNPs and AuNRs with varying native caps.[27,43−46] To reduce the time required for promoting the coordination of thiol-modified alkyls or biomolecules onto gold surfaces, a few groups have used external stimuli to accelerate the process. In one study, Liu and co-workers reported that more dense thiol-appended DNA layers can be attached onto AuNPs when the mixed materials are rapidly immersed in dry ice for 2 min.[47] In another study, Zharnikov and co-workers have shown that irradiating a self-assembled monolayer (SAM), immersed with a solution of disulfide molecules with an electron beam, can promote the formation of mixed monolayer coverage.[48] In a third study, Sahli and co-workers observed the buildup of saturated SAMs of LA-appended molecules on Au electrodes in less than 10 min when a moderate cathodic potential was applied.[49] Our group has shown that UV-irradiation, using a band centered at 350 nm, of hydrophobic semiconducting nanocrystals (ZnS-overcoated quantum dots, QDs), mixed with lipoic acid ligands in their stable oxidized form, promotes *in situ* rapid ligand exchange; additionally, reduced amounts of ligands are required. We should note that lipoic acid in its oxidized form cannot coordinate onto QDs.[50,51] Inspired by these results, Velders and co-workers have recently reported that ligand substitution and phase transfer of oleylamine−AuNPs (of different sizes) to aqueous media using LA molecules can be implemented using *in situ* UV-irradiation for 30−60 min.[52]

Here we demonstrate the effectiveness of the photoligation strategy to cap a series of lipoic acid-based ligands onto several gold nanocolloids with varying shape and size. We explore the effects of varying a few key parameters (e.g., irradiation time and ligand concentration) on the quality of the resulting materials by comparing properties such as optical spectra, hydrodynamic size, and colloidal stability. We find that photoligation promotes substantially more rapid ligand substitution and phase transfer than the conventional route (without UV-irradiation): ∼30 min vs ∼14 h on average. Additionally, this route requires about 1 order of magnitude less ligands, while providing biocompatible nanoparticles with high colloidal stability and preserved photophysical properties. ^{1}H NMR and FT-IR measurements provide evidence for a complete substitution of the native cap with the LA-R ligands. We combine our findings with literature data to provide thermodynamic insights into how photochemical reduction of the lipoic acid groups and *in situ* ligand substitution make photoligation rapid and effective for coating a variety of Au nanocolloids.

RESULTS AND DISCUSSION

Testing the effectiveness of the photoligation strategy to promote coating and stabilization of gold nanocolloids with LA-R ligands was motivated by the desire to shorten the time required for a full ligand exchange, reduce the amount of ligands used, and ultimately provide high quality hydrophilic materials. This was also inspired by two experimental observations relating to the photophysics of the dithiolane ring (in LA) and the remarkable effectiveness of the photoligation strategy applied to luminescent QDs. (1) Given its structure, the five-membered dithiolane ring exhibits a well-defined absorption band centered at 335 nm. Irradiating a solution of LA or any LA-R with a UV signal within that absorption band induces fission of the disulfide bond (LA → LA*) and yields compounds that are highly reactive toward the surfaces of certain metal-rich nanocolloids.[51,53] As such, we have shown that photoligation of several LA-R ligands (monomeric or polymeric in nature) onto ZnS-overcoated QDs is rapid and yields stable and highly luminescent hydrophilic materials.[50,51,54,55] (2) We have found that LA-R* compounds exhibit higher competitive binding onto AuNPs, preassembled with polyhistidine−mCherry proteins, with a dissociation constant, K_d, that is ∼3-fold smaller than the one measured for their oxidized LA-R counterparts.[56] On the basis of these observations, we reasoned that photoligation of Au nanocolloids with LA-R ligands could provide tangible benefits and yields high quality materials for use in biomedicine and other applications.

The photoligation strategy was applied to coat several sets of gold colloids with LA-based ligands, as schematically illustrated in Figure 1. The gold nanocolloids include the following: (1) Oleylamine-stabilized AuNPs ($2R \simeq 10$ nm, from TEM), grown by using the method originally developed by Osterloh and co-workers.[57,58] (2) Two sets of citrate-stabilized spherical

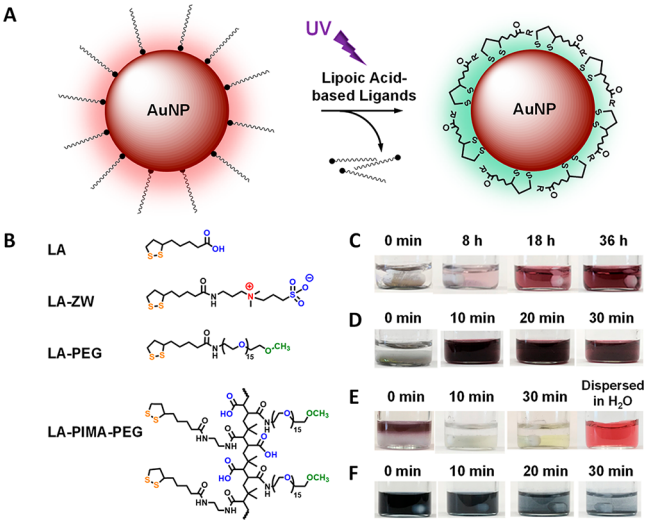

Figure 1. (A) Schematic representation of the *in situ* photoligation procedure applied to cap exchange gold nanoparticles with lipoic acid (LA)-based ligands. (B) Chemical structure of four representative ligands used: LA, LA-ZW, LA-PEG, and LA-PIMA-PEG. (C−F) White light images showing visual progression of the AuNP-plus-ligand mixtures during ligand substitution. (C) Conventional incubation: mixing oleylamine−AuNPs precipitate with lipoic acid in DMF promotes slow dispersion and homogenization of the NPs achieved after 36 h of incubation. (D) The same reaction as in panel C shows that homogenization is reached within 30 min when using a UV flux. (E) Photoirradiation of oleylamine−AuNPs dispersed in hexane with a LA-ZW ligand in methanol (two-phase configuration) for 30 min yields phase transfer of the NPs from hexane to methanol, coupled with precipitation. A homogeneous water dispersion of the LA-ZW-AuNPs following processing is also shown. Note that incubation without UV-irradiation produces a turbid mixture of aggregate materials that cannot be processed. (F) UV-irradiation of PVP-AuNSs with LA-ZW in methanol produces macroscopic aggregation of the nanocrystals, reflecting a complete ligand exchange coupled with loss of LA-ZW-AuNS affinity to methanol.

https://dx.doi.org/10.1021/acs.chemmater.0c02482
Chem. Mater. 2020, 32, 7469−7483

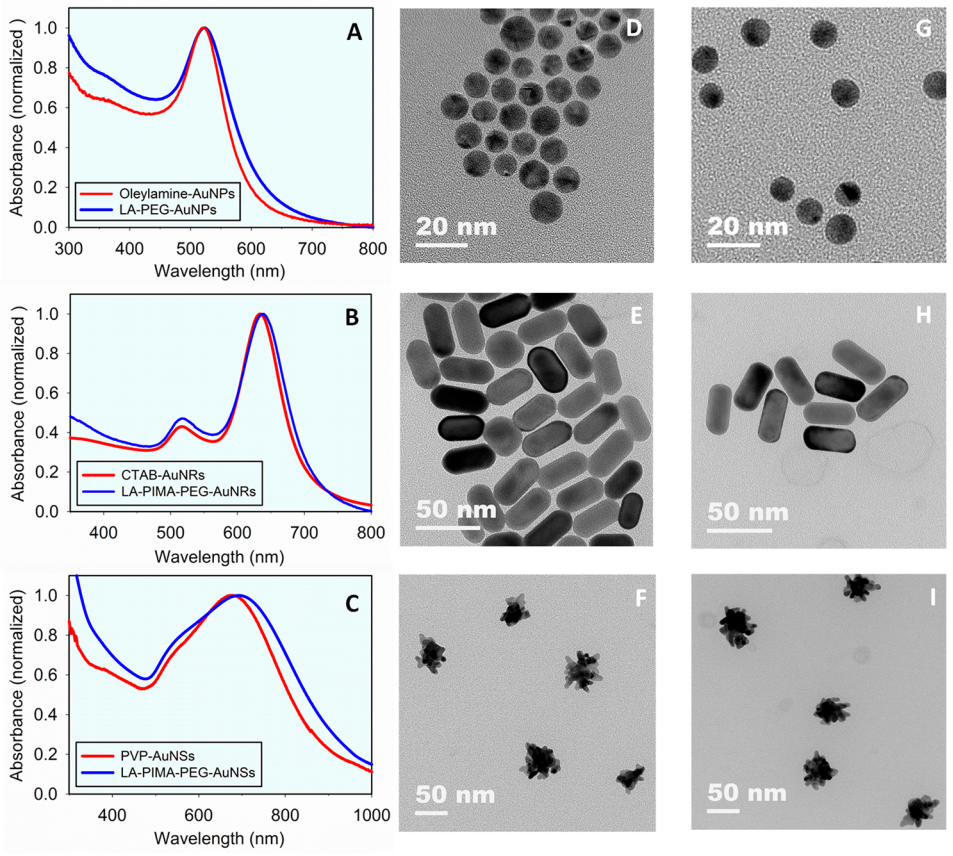

Figure 2. (A–C) Representative absorption spectra collected from AuNP, AuNR, and AuNS dispersion, as-grown (red profiles) and after photoligation with either LA-PEG or LA-PIMA-PEG (blue profiles). (D–F) TEM images of the as-grown gold nanostructures, showing oleylamine–AuNPs ($2R \sim 9.5$ nm) in (D), CTAB–AuNRs ($L \times D = 45$ nm $\times$ 19 nm) in (E), and PVP–AuNSs ($d_{core} \times l_{tip} \sim 25$ nm $\times$ 12 nm) in (F). TEM images of the corresponding photoligated gold nanocolloids are shown in panels G, H, and I. No changes in the dimensions of the various materials were measured after ligand exchange.

AuNPs. One set was grown by using $NaBH_4$ reduction ($2R \sim 5$ nm, from TEM)[59−61] and the other by using the high-temperature aqueous growth conditions initially developed by Turkevich ($2R \simeq 13$ nm, from TEM).[62−65] (3) CTAB-stabilized AuNRs with length $L = 45$ nm and cross-sectional diameter $D = 19$ nm (from TEM), which were prepared following the refined seed-mediated growth method introduced by the groups of Murphy and Murray and stabilized with hexadecyltrimethylammonium bromide (CTAB).[27,66−69] (4) Polyvinylpyrrolidone (PVP)-coated AuNSs ($\overline{d}_{core} \times \overline{l}_{tips} = 25 \times 12$ nm, from TEM), grown following the route introduced by Liz-Marzán and co-workers.[70] TEM characterization of the gold colloids is summarized in Figure 2. Three sets of LA-modified ligands were used, including two molecular scale compounds (i.e., LA-PEG_{750}-OCH_3 which will be termed LA-PEG and LA-ZW), synthesized by following literature protocols,[71,72] and a multicoordinating polymer (i.e., LA-PIMA-PEG); the latter was synthesized via nucleophilic ring-opening reaction between a low-molecular-weight poly(isobutylene-*alt*-maleic anhydride), PIMA, copolymer and a mixture of amine-LA and amine-PEG_{750}-OCH_3 nucleophiles.[27,54,73]

Photomediated ligand exchange of the gold colloids was performed (*in situ*) by using either one- or two-phase reaction, depending on whether the starting materials were hydrophilic or hydrophobic in nature and on the solubility of the ligand. A few representative examples are described below. Photoligation of the as-grown oleylamine–AuNPs with LA-ZW or LA-PEG ligands was performed by using a two-phase reaction (hexane and methanol), which allows visual tracking of the phase transfer combined with easy purification, as shown in Figure 1E. We should note that photoligation of the oleylamine–AuNPs with LA-PIMA-PEG is easier and more efficiently implemented using one-phase reaction in $CHCl_3$ or THF. We would also like to stress that photoinduced ligand exchange and phase transfer are particularly advantageous for LA-ZW ligands, since the conventional incubation route does not provide homogeneous aggregate-free dispersions.[27] Photoligation of water-dispersible citrate–AuNPs was performed under one aqueous phase conditions for all the ligands. Photoligation of CTAB-AuNRs with LA-PEG or LA-PIMA-PEG was also performed by using one aqueous phase. Nonetheless, photoligation of the AuNRs with LA-ZW required a slightly modified protocol. It was performed in two steps. First, the as-grown CTAB-AuNR dispersion was mixed with poly(4-styrenesulfonic acid) sodium salt, PSS, for 1 h and then precipitated by centrifugation. The NR pellet was redispersed in water, mixed with the ligand, and then UV-irradiated. The PSS step circumvents aggregation problems, which occur if the CTAB-NRs are directly mixed with LA-ZW. Photoligation of PVP-AuNSs was performed by using the one-phase reaction in methanol. In particular, we found that irradiation of PVP-AuNSs mixed with LA-ZW in methanol produces precipitates of the newly ligated AuNSs, allowing a

https://dx.doi.org/10.1021/acs.chemmater.0c02482
Chem. Mater. 2020, 32, 7469−7483

Table 1. Effects of Varying the UV-Irradiation Time and Ligand Concentration on the UV−Vis Absorption Profile and Hydrodynamic Size Measured for Dispersions of LA-PEG-Stabilized AuNPs, Prepared Starting with Oleylamine (OLA)-Capped Nanocrystals[a]

	20 min photoligation			30 min photoligation			40 min photoligation			control (18 h, no UV)		
excess of ligand[b]	SPR	R_H	PDI	SPR	R_H	PDI	SPR	R_H	PDI	SPR	R_H	PDI
1200000	522	10.9	0.23	523	10.6	0.10	522	10.2	0.11	522	9.9	0.15
120000	521.5	11.9	0.20	521.5	10.7	0.11	523	10.9	0.10	522	9.6	0.18
12000	523	12.6	0.18	522	10.1	0.07	521.5	10.7	0.10	N	N	N
2400	N	N	N	N	N	N	N	N	N	N	N	N

[a]Data from conventional ligand exchange are also shown. "N" indicates a failed reaction, where irreversible aggregation was observed. [b]Equal to [c(LA-PEG)]/[c(OLA-AuNPs)]. Data from other combinations of gold colloids and LA-containing ligands are provided in Table S1.

convenient route to isolate the products, as illustrated in Figure 1F. This is attributed to the drastic change in the solubility of free vs colloid-bound LA-ZW in methanol.[71] Additional details are provided in the Experimental Section and the Supporting Information.[74−76]

Initial experiments focused on identifying the optimal conditions for providing colloidally stable AuNPs. Then, dispersions of the various Au colloids were characterized by using optical absorption, transmission electron microscopy (TEM), and dynamic light scattering (DLS). In addition, FT-IR, 1-D ^{1}H NMR, and 2-D diffusion ordered spectroscopy (DOSY) measurements were employed to verify whether or not a complete removal of the native ligands is achieved by using the photoligation strategy. Their stability was evaluated under various conditions, including dispersions in growth media (rich in excess ions), sodium cyanide digestion test, and destabilization triggered by excess dithiothreitol (DTT).

Optimization of the Photoligation Conditions. The optimal irradiation time and amount of excess ligands needed for achieving complete ligand substitution were evaluated by tracking the absorption spectra, with a focus on the SPR band, and probing changes in the intensity vs hydrodynamic radius histograms (acquired from DLS measurements). These profiles are strongly affected by heterogeneity in the colloid dispersions such as aggregate formation.

First, we varied the excess amount of LA-PEG with respect to the concentration of the NPs from 1200000× to 2400× and the irradiation time from 20 to 40 min.[50] We note that 1200000× molar excess of ligands corresponds to ∼400× compared to the concentration of surface Au atoms (for oleylamine−AuNPs with $2R$ = 10 nm).[28] Further experimental details are provided in the Supporting Information. The data collected from DLS measurements (summarized in Table 1) suggest that excess ligand of 12000× or larger combined with irradiation time of 20−40 min yielded homogeneous dispersions with SPR values that are essentially identical with the starting materials (≃522 nm) along with R_H values of 10.5 ± 0.5 nm. Nonetheless, the DLS data show that the lowest PDI values (0.07−0.11) are measured when the irradiation time is 30 or 40 min. Photoligation using 20 min UV-irradiation also yields a single peak for the intensity vs R_H profile, albeit a PDI of ∼0.2−0.23, implying that shorter irradiation time is likely to produce a slightly higher heterogeneity in the NP dispersion. In comparison, materials prepared by using the conventional incubation strategy (for ∼18 h) require excess amount of ligands of 120000× or larger to provide similar profiles, in agreement with previous results from our group.[28] We should note that photoligation of citrate−AuNPs with LA-PEG also yielded homogeneous dispersions under all conditions tested (both time and excess ligands), albeit slightly higher PDI values were measured (see Table S1); this may be attributed to the higher size dispersity of the native NPs. Plots of the autocorrelation function, $\ln(g^{(1)})$ vs τ, along with the intensity vs R_H profiles extracted from DLS measurements for dispersions prepared starting from oleylamine- or citrate-stabilized AuNPs are provided in the Supporting Information (Figure S1).

Next, we determined the optimal irradiation time required for ligand exchange of anisotropic gold nanostructures (e.g., nanorods and nanostars) using 1200000× excess LA-PEG; this corresponds to molar excess with respect to surface Au atoms of 40×, taking into account the larger surface area of NRs compared to NPs (see Figure S2). Here, too, we found that ligand exchange is complete within ∼30 min of UV-irradiation. Similarly, 30 min irradiation of PVP-AuNSs and LA-ZW mixture in methanol, at similar molar excess, yielded complete ligand substitution, which manifests in the macroscopic AuNS aggregation shown in Figure 1F. These incubation times are consistent with previous data, where a near-complete photochemical transformation of LA derivatives dissolved in various solvents can be achieved by using UV-irradiation for ∼25−30 min.[51−53]

Overall, the above data allow us to conclude that UV-irradiation for ∼30 min, using either one- or two-phase configuration, achieves full ligand substitution of several Au nanocolloids, regardless of their exact structure, the architecture of the ligand, or solvent used. Additionally, the photoligation strategy requires substantially fewer ligands than the conventional route (performed without UV exposure). Indeed, conventional ligand exchange of CTAB-AuNRs using LA-PEG requires ∼1 order of magnitude larger excess ligands to provide colloidally stable materials (Table S1). Consequently, photoligation drastically shortens the incubation time required and reduces the excess ligands needed to prepare biocompatible colloids with high photophysical and colloidal properties compared to the conventional incubation route.

Characterization of the Photoligated Gold Nanocolloids. *UV−Vis Absorption, TEM Size and Shape Measurements.* These measurements were used to assess the effects of photoligation on the integrity of the nanocrystals and homogeneity of the corresponding dispersions. Gold colloids exhibit a unique SPR band at ∼520 nm, along with size- and shape-dependent second feature that spans the red to NIR region of the optical spectrum. Figure 2A−C shows that the optical absorption profiles collected from these nanocrystals before and after photoligation with the LA-based ligands are essentially identical, implying that the photophysical integrity of the gold nanocolloids is unaffected by the ligand exchange process. TEM data corroborate this result. Indeed, the three

https://dx.doi.org/10.1021/acs.chemmater.0c02482
Chem. Mater. 2020, 32, 7469−7483

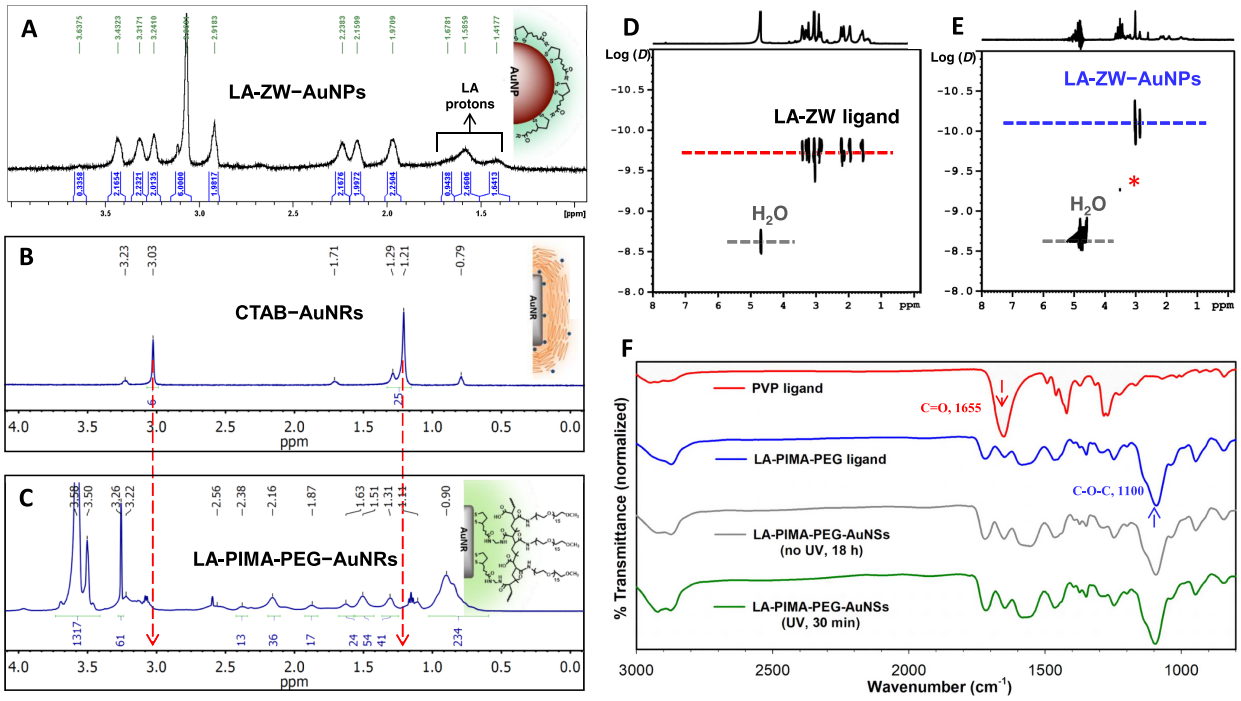

Figure 3. ^{1}H NMR spectra collected from (A) LA-ZW-AuNPs prepared via photoligation starting with oleylamine−AuNPs, (B) as-grown CTAB-AuNRs, and (C) AuNRs photoligated with LA-PIMA-PEG ligands. D_2O was used for all samples. DOSY contour spectra acquired from (D) LA-ZW ligand solution ($D = 1.7 \times 10^{-10}$ m^2/s) and (E) LA-ZW-AuNP dispersion ($D = 3.4 \times 10^{-11}$ m^2/s). The signal at 4.47 ppm is associated with $D \simeq 1.8 \times 10^{-9}$ m^2/s corresponds to H_2O impurities in the medium. DOSY data were collected at room temperature ($T = 298$ K). (F) Representative FT-IR spectra collected from pure PVP polymer (red) and LA-PIMA-PEG ligand (blue) along with two sets of LA-PIMA-PEG-AuNSs, one set prepared by using a conventional incubation (gray curve) and the other prepared via photoligation (green curve). Additional spectroscopy data are provided in Figures S4−S6.

representative sets of images acquired for each type of colloid, either as-prepared or after photoligation with the ligands, indicate that the nanocrystals have fully preserved their size and shape during ligand substitution (see Figure 2, panels D−F and G−I). Similar data were collected from the gold nanocolloids photoligated with the molecular scale ligands (data not shown). These findings are complemented with DLS measurements introduced above for spherical nanocolloids, which are very sensitive to aggregate built up in the dispersion.[77] Semilogarithmic plots of the autocorrelation profiles ($\ln(g^{(1)})$ vs τ), together with the corresponding intensity vs R_H histograms, extracted from $g^{(1)}(\tau)$ by using the Laplace transform, indicate that the dispersions are homogeneous and free of any aggregates. Only a slight increase in R_H and PDI values is measured after surface coatings with the various new ligands. For instance, our experiments yield $R_H \sim 7.8$ nm for oleylamine−AuNPs and $R_H \sim 8.6$, 10.5, and 13.3 nm after photoligation of the NPs with LA-ZW, LA-PEG, and LA-PIMA-PEG, respectively (see Figure S1 for scattering profiles). The larger hydrodynamic radii measured after ligand substitution reflect the more complex architecture of the new coatings; this manifests in more pronounced effects of hydrodynamic interactions, as they contribute to the measured mobility of the nanocolloids compared to the starting materials. We should note that these radii are consistent with our previous data collected for AuNPs prepared by using the conventional incubation method.[27]

Characterization of the Surface-Bound Ligands. To verify whether or not complete removal of the native cap has taken place under the conditions used and identify the ligand molecules in the final coating, we have performed solution-phase ^{1}H NMR, FT-IR, and fluorescence measurements for select representative photoligated nanocolloids. We note that the fluorescence measurements are limited to Au nanostars.

(i) The use of NMR spectroscopy techniques to probe the surface coating of inorganic nanocolloids has recently gained much interest and yielded valuable information with respect to both ligand structure, stoichiometry, and dynamics of ligand binding and desorption rates.[78−81] Figure 3A−C shows representative solution phase ^{1}H NMR spectra collected from dispersions of AuNPs photoligated with LA-ZW (starting with oleylamine−NPs), AuNRs as-grown (CTAB-capped), and after photoligation with LA-PIMA-PEG. The spectrum in Figure 3A shows three broad resonances at 1.3−1.7 ppm, assigned to the lipoic acid protons, and a well-defined peak at 3.1 ppm, ascribed to the methyl groups in the sulfobetaine moieties. Importantly, the proton signatures emanating from oleylamine protons (e.g., $-C\underline{H}_2-NH_2$ at 2.5 ppm) are conspicuously absent from the data acquired from the LA-ZW-AuNP dispersion. The spectra collected from dispersions of CTAB-AuNRs and LA-PIMA-PEG-AuNRs, shown in Figure 3B,C, indicate that the well-defined signatures ascribed to the CTAB molecules in the native NRs (at 1.2 and 3.0 ppm) are absent from the spectrum collected from the polymer-capped AuNRs. This confirms that the native cap has been completely removed during photoligation and purification steps. The above ^{1}H NMR spectra are supplemented with DOSY-NMR experiments. This technique relies on differences in the Brownian diffusion coefficients, corresponding to specific proton signatures

https://dx.doi.org/10.1021/acs.chemmater.0c02482
Chem. Mater. 2020, 32, 7469−7483

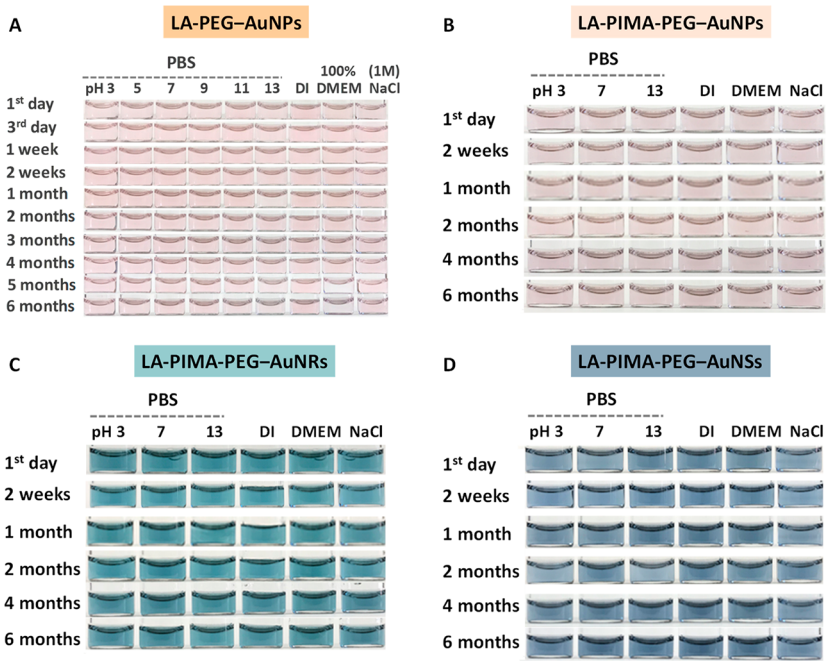

Figure 4. Long-term colloidal stability tests, including pH changes in various PBS buffers, DI water, cell growth media (100% DMEM), and in ion-rich dispersions (1 M NaCl), applied to representative dispersions of (A) LA-PEG-AuNPs (3 nM, 300 μL). (B) LA-PIMA-PEG-AuNPs (3 nM, 300 μL). (C) LA-PIMA-PEG-AuNRs (0.5 nM, 300 μL). (D) LA-PIMA-PEG-AuNSs (0.5 nM, 300 μL). Samples were prepared via photoligation and stored at 4 °C. Oleylamine-AuNPs were used in (A,B). Tests on other samples are provided in the Supporting Information (Figure S7).

in a spectrum, to differentiate between the features associated with either surface-coordinated or freely moving ligands in the sample.[81−83] Additionally, surface-bound ligands exhibit weakening and broadening of the NMR features compared to free molecules, and they experience slower diffusion properties; free moving ligands exhibit much faster translational diffusion, in comparison.[83,84] Figure 3D,E shows two DOSY contour plots collected from a solution of free LA-ZW and a dispersion of LA-ZW-AuNPs both in D_2O. These plots show that only one diffusion coefficient is measured for each sample. In addition, $D_{\text{LA-ZW-AuNP}}$ measured from the NP dispersion is ∼5-fold smaller than the one measured from LA-ZW solution ($D_{\text{LA-ZW}}$), which proves that only surface-coordinated LA-ZW ligands contribute to the NMR spectrum collected from photoligated and purified NPs. We note that the spectra also show the presence of a much faster diffusion coefficient associated with the features at ∼4.7 ppm, ascribed to H_2O impurities in the sample.

(ii) Figure 3F shows select representative FT-IR spectra acquired from LA-PIMA-PEG-AuNSs, prepared either via photoligation or the conventional incubation method, side-by-side with spectra collected from the pure PVP and LA-PIMA-PEG (as controls). The spectrum collected from the LA-PIMA-PEG-AuNS sample (green profile) shows a weak signature at 1655 cm^{-1} and a strong peak at 1100 cm^{-1}, which are respectively ascribed to the stretching modes of the amide C═O groups along the polymer chain and C−O−C groups in the PEG blocks of the polymer coat.[73] This spectrum is identical with the one collected from a sample of polymer−AuNSs prepared by using conventional ligation (compare green and gray profiles). Additionally, the strong peak at 1655 cm^{-1} measured for the pure PVP sample (red profile) and ascribed to the C═O stretching mode of the vinylpyrrolidone rings has been replaced with a weaker one emanating from ligands in the LA-PIMA-PEG-AuNS coating.

(iii) Complete substitution of the PVP coating on the nanostars could also be determined from fluorescence measurements. PVP was shown to interact with the gold surfaces through either amine-N and/or carbonyl-O electron donors.[85] Because of the weak intrinsic fluorescence properties of PVP polymers, the starting PVP-AuNSs exhibit broad fluorescence with a maximum at ∼400 nm (see Figure S3).[86] Negligible fluorescence was measured for dispersions of photoligated LA-PEG-AuNSs, in comparison.

Cumulatively, these observations provide strong evidence that the native cap (e.g., oleylamine, citrate, CTAB, and PVP molecules) have been fully substituted with the various LA-modified ligands using the photoligation strategy. Additional data showing UV−vis absorption profiles and ^{1}H NMR spectra collected from CTAB-stabilized AuNRs (i.e., as-prepared) and after ligation with molecular scale ligands (e.g., LA-ZW) are provided in the Supporting Information (Figures S4−S6).

Colloidal Stability Tests. The tests have been performed to assess the ability of the photoligation route to provide nanocolloids that can perform well under conditions of great relevance to biology (namely, pH changes, excess NaCl, and in the presence of cell growth media). The tests also probe how architecture, coordination affinity and nature of the hydrophilic motifs in the ligand used would affect the ability of the coating to protect the inorganic cores against chemical digestion by sodium cyanide, known to exhibit high reactivity toward metals including gold, and competition from DTT, a redox small molecule with high affinity for gold surfaces.[27,28] The data were compared to colloids prepared by using conventional incubation (under UV-free conditions).

https://dx.doi.org/10.1021/acs.chemmater.0c02482
Chem. Mater. 2020, 32, 7469−7483

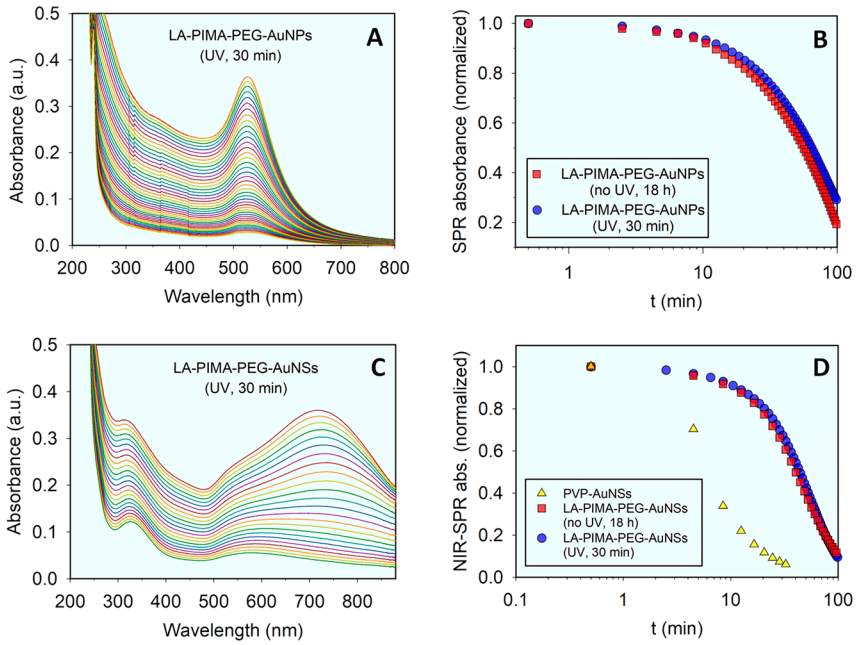

Figure 5. NaCN digestion tests. Shown are (A) time progression of the absorption profiles collected from photoligated LA-PIMA-PEG-AuNP dispersions (12.5 nM, 600 μL along with 50 mM NaCN). (B) Time-dependent progression of the normalized optical density at ∼520 nm, extracted from data in (A). The red squares correspond to a conventional sample, while the blue circles are data from a photoligated sample, t_D ∼ 80 min for both cases. (C) Time progression of the absorption profiles collected from photoligated LA-PIMA-PEG-AuNS dispersions (0.35 nM, 600 μL along with 50 mM NaCN). (D) Time-dependent progression of the normalized optical density at ∼715 nm, extracted from data in (C); conventional ligation (red squares) and photoligation (blue circles), t_D ∼ 60 min. The yellow triangles are data from PVP−AuNS dispersion, wth t_D ∼ 7.3 min. Results from other samples and test conditions are summarized in Table 2.

Effects of pH, Excess Ions, and Cell Growth Media. For this, two sets of LA-PEG-AuNPs were prepared: one set using photoligation of oleylamine-AuNPs and the other using citrate-AuNPs. Dispersions of LA-PEG-AuNPs obtained via the conventional incubation route were stable under all tested conditions for at least 6 months of storage (data not shown).[27,28] Figure 4A shows white light images of LA-PEG-AuNP dispersions in PBS at pH ranging from 3 to 13, dispersions containing 1 M NaCl, and in 100% DMEM, tracked over a period of 6 months of storage. The dispersions exhibited excellent colloidal stability under all those conditions, with no degradation or aggregation buildup; only the dispersion in DMEM showed a slight color change after 6 months. Essentially identical stability data were collected for AuNPs photoligated with LA-PIMA-PEG (Figure 4B) or LA-ZW ligands, starting with the same oleylamine-coated materials (see Figure S7). Additional data from the same test using LA-PEG-AuNPs prepared via photoligation starting with citrate-stabilized nanocrystals show similar behavior; this contrasts with immediate aggregation of the starting citrate-AuNPs observed in the presence of 1 M NaCl (see Figure S7). However, when these tests were applied to AuNRs and AuNSs photoligated with LA-ZW, LA-PEG, or LA-PIMA-PEG, only the polymers promoted long-term stability across all explored conditions (see Figure 4C,D). Rather limited stability was measured for these high-order nanostructures ligated with molecular scale ligands (LA-ZW or LA-PEG) (see Figure S7). These findings are consistent with data collected from Au nanoparticles, nanorods, and nanoshells coated with the LA-based ligands by using overnight incubation, albeit with higher molar excess of the oxidized form.[27] This indeed confirms that the photoligation strategy, in particular by using the high coordination polymers, yields high quality colloids across a wide range of conditions.

NaCN Digestion Tests. We have tested the ability of the surface coatings to protect the gold nanostructures against cyanide (CN^-) digestion and compared the rates of digestion measured for photo- and conventionally ligated samples, side by side. Given their small size and strong ionic nature, CN^- ions can diffuse through the ligand barriers and form gold complexes with surface atoms, progressively etching away the nanocrystals.[27,28,87] However, the rate of digestion depends on the binding affinity and lateral extension of the ligand coating used. For the various Au nanocolloids, we used nanocrystal concentration corresponding to an optical density at the SPR value of ∼0.35 and fixed the NaCN concentration at 50 mM; these conditions have been reported to achieve complete digestion within 2 h for similar size NPs.[27,28]

Representative time-dependent progression of the absorption spectra collected from photoligated LA-PIMA-PEG-AuNP and LA-PIMA-PEG-AuNS dispersions are shown in Figure 5A,C. We then assessed the digestion time by fitting the profiles for the decrease in the SPR intensity (at ∼520 nm for AuNPs and at 715 nm for AuNSs) vs time to a single-exponential decay function:[88]

$$A = A_0 e^{-t/t_D} \quad (1)$$

where A_0 is the initial absorbance value and t_D is the digestion time. Figure 5A,B shows that LA-PIMA-PEG-AuNPs prepared by using either photoligation or the conventional long incubation route exhibit nearly identical digestion profiles, with t_D ∼ 80 min. Similarly, AuNS dispersions prepared by using either photoligation for 30 min or overnight incubation with LA-PIMA-PEG also show indistinguishable digestion

https://dx.doi.org/10.1021/acs.chemmater.0c02482
Chem. Mater. 2020, 32, 7469−7483

Table 2. Values for the Digestion Time, t_D, Extracted from the NaCN Digestion Tests Applied to the Various LA-Based Cap Used to Stabilize the Gold Colloids; Estimates of Several Other Relevant Parameters Including Molar Absorption Coefficients, Concentration, and Number of Surface Atoms

							t_D (min) (photoligation)			t_D' (min)[c] (conventional reaction)		
dimensions of NP (nm)	ε (M^{-1} cm^{-1})	N_{S-Au}[a]	optical density (0.5 cm)	[Au colloids] (nM)[b]	[NaCN] (mM)	$[CN^-]/N_{S-Au}$ ratio	LA-ZW	LA-PEG	LA-PIMA-PEG	LA-ZW	LA-PEG	LA-PIMA-PEG
AuNP: 9[d]	5.6×10^7	~3000	0.35	12.5	50	~1333	14.6	39.7	80.6	15.5	42.7	75.7
AuNR: 42 × 19	2.8×10^9	~31646	0.35	0.25	50	~6320	18.2	33.0	62.3	9.1	27.5	64.5
AuNS: 25 × 12	2.0×10^9	~33127	0.35	0.35	50	~4312	23.3	71.5	57.8	29.0	80.0	59.0

[a]Estimated number of surface gold atoms per NP (N_{S-Au}).[28] [b]A smaller concentration of Au nanocolloids is used to compensate for the larger number of surface and total gold atoms per NP. [c]t_D(CTAB-AuNRs) is ~3.3 min; t_D(PVP-AuNSs) is ~7.3 min. [d]Prepared starting from oleylamine-AuNPs.

profiles with $t_D \sim 60$ min (see Figure 5C,D). A summary of the conditions used for the various combinations of nanocolloids and ligands used along with the extracted values for t_D is provided in Table 2. The data show that the trends as well as the values for t_D, obtained for the various nanocrystal-ligand combinations, prepared either via photoligation or conventional incubation are comparable. Additionally, the data acquired from the AuNPs and AuNRs, prepared by using the conventional route, are comparable to those previously reported by our group.[20,27,28] Figure 5D also shows that the digestion times measured for newly coated nanostars (e.g., $t_D \sim 23-71$ min depending on the ligand structure) are significantly larger than the one extracted for the native PVP-AuNS dispersions ($t_D \sim 7.3$ min).

A closer examination of the data also shows that the digestion kinetics for Au nanostars are substantially slower in the presence of the LA-PEG cap than those measured for LA-PIMA-PEG and LA-ZW coatings (see Table 2). This contrasts with the data collected for spherical NPs and anisotropic NRs. The less protective polymer coatings for the AuNS materials may be attributed to their uneven surface morphology combined with the natural swelling of the polymer chains.[89] Indeed, swelling of the individual chains affects how these ligands "adhere" onto the complex surface morphology of these colloids, reducing the polymer coordination affinity, compared to mono-LA-PEG ligands. Conversely, given the dual cationic/anionic nature of the zwitterion motif, LA-ZW coating does not provide strong shielding but rather facilitates CN^- ion penetration near the colloid surfaces. Difference in the digestion kinetics between PEG and zwitterion coatings have also been measured for AuNPs.[27]

DTT Competition Tests. This test is particularly suitable for probing the strength of the ligand coordination to metal colloid surfaces and its ability to impart long term colloidal stability under strong reducing conditions. Given their small size, these dithiol molecules can easily diffuse through the coating layer and directly interact with the surface of the nanocrystals. At high concentration and in the presence of excess NaCl, DTT molecules can competitively displace coordinated ligands. However, because they do not present solubilizing motifs, they tend to destabilize the nanocolloid dispersion, thus causing progressive aggregation. The rate of aggregation is accelerated when the affinity of native cap to the nanocrystal is low, and *vice versa*.[27,28] The destabilization process manifests in a progressive loss of the plasmon features of the nanocolloid dispersions due to the close proximity between nanocolloid surfaces within aggregates.

For this DTT test, we focus on the stability of gold nanorods as a representative system because they have large surface areas, and stabilization of the platforms is strongly dependent on the coordination affinity and nature of the ligands used. We also probed dispersions of AuNRs stabilized via photoligation with polymer or monomer ligands and compared the data to control samples prepared via overnight incubation (i.e., no UV). Figure 6A shows the time progression of the absorption

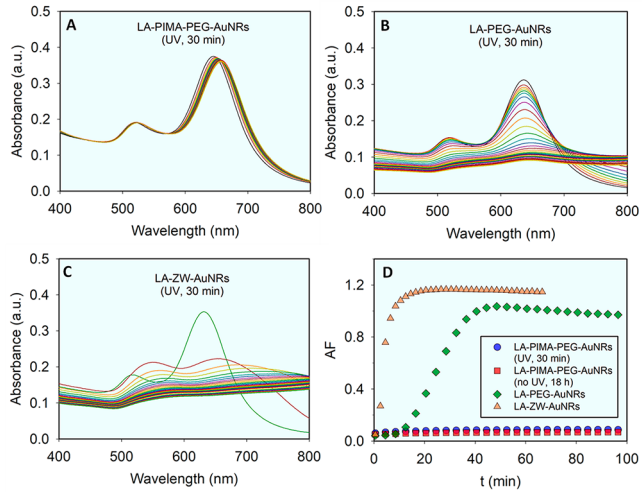

Figure 6. DTT competition tests. Time progression of the absorption spectra collected from various dispersions of LA-R-AuNRs prepared via photoligation (0.25 nM, 600 μL) in the presence of 1 M DTT and 400 mM NaCl. (A) LA-PIMA-PEG-AuNRs. (B) LA-PEG-AuNRs. (C) LA-ZW-AuNRs. (D) Profiles for AF vs time extracted from the data shown in (A–C). No aggregation was observed for the polymer-capped AuNRs. The profiles acquired for NRs ligated with monomeric LA-PEG or LA-ZW reflect rapid aggregation buildup. The rise in AF values is more pronounced for zwitterion capping, nonetheless. Note that the data from the sample of LA-PIMA-PEG-AuNR dispersion prepared via conventional incubation (control) also show no sign of aggregation buildup (see Figure S8).

spectra collected from dispersions of AuNRs ligated with LA-PIMA-PEG, which contain 1 M DTT and 400 mM NaCl. The spectra collected from dispersions of AuNRs photoligated with either LA-ZW or LA-PEG (molecular scale ligands) for 30 min under the same conditions are shown in Figure 6B,C. The changes in the absorption profile, namely, the decay of the longitudinal SPR peak with time, can be used to draw conclusion about resistance of the capping to DTT competition by using an aggregation factor, AF, defined by

https://dx.doi.org/10.1021/acs.chemmater.0c02482
Chem. Mater. 2020, 32, 7469–7483

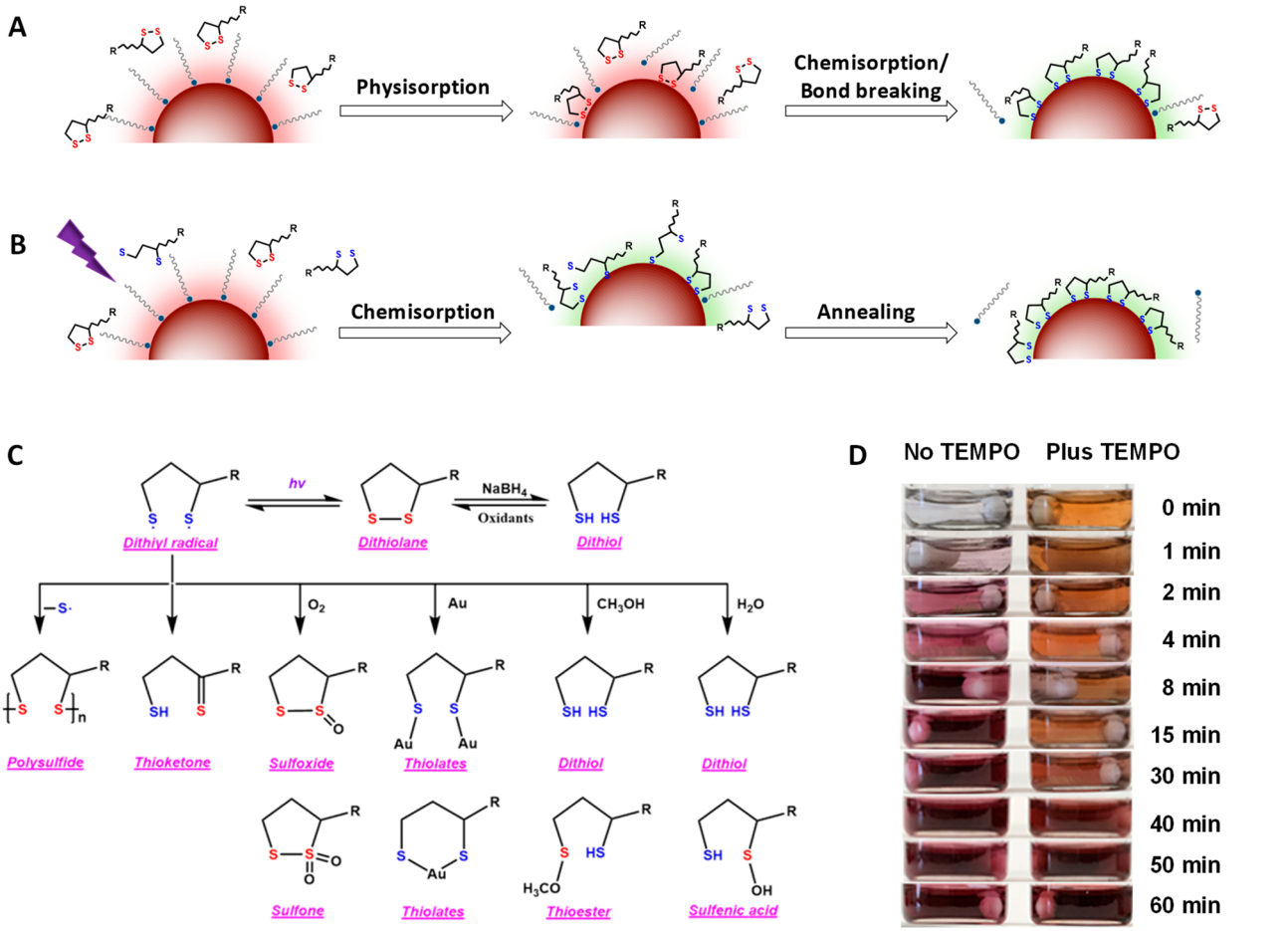

Figure 7. Proposed mechanistic model for(A) conventional ligand exchange of AuNPs with LA-R. The second step involves a "S−S" bond breaking event. (B) Photoligation promotes cleavage of the "S−S" bond *in situ*, where the resulting radicals and sulfhydryl-appended species exhibit high reactivity to the gold colloid surfaces. Subsequently, a fraction of single thiol-attached compounds are substituted with bidentate ligands during annealing. (C) Schematic description of certain photochemical transformations of LA-based ligands under UV-irradiation. Ring dissociation leads to the formation of dithiyl radicals, which may undergo protonation, polymerization, oxidation, or complexation. Possible modes of hydrogen atom abstraction by the diradicals from protic solvent molecules (e.g., methanol and water) leading to the formation of thiol products and other byproducts are shown. (D) Time-lapse white light images showing progression and homogenization of AuNP dispersions (starting with oleylamine−AuNPs) during photoligation with lipoic acid in DMF. The shown dispersions are without (left column) and with radical trapping agent TEMPO (right column); molar ratio of TEMPO:LA = 8 is used. Note that the TEMPO solution is naturally orange.

the ratio between the absorbance at 800 nm to that at the longitudinal SPR:[27]

$$\mathrm{AF} = \frac{\mathrm{Abs}_{800}}{\mathrm{Abs}_{635}} \qquad (2)$$

Figure 6D shows that the measured AF for the photoligated LA-PIMA-PEG-AuNRs stays near zero over the test period. Essentially identical data were acquired by using NR dispersions prepared via conventional ligand exchange (see Figure S8 and ref 27). In contrast, when the AuNRs are photoligated with the monomeric LA-ZW and LA-PEG, which have lower coordination affinity, the test shows faster changes in the absorption profiles, combined with an increasing AF with time, albeit slightly more pronounced for the zwitterion ligand coating. Comparing the kinetic of the DTT destabilization data extracted for the three coatings indicates that the higher coordination affinity afforded by the polymer ligands imparts better resistance to DTT competition than ligands with lower coordination such as LA-ZW and LA-PEG. We should note that although LA-ZW and LA-PEG have the same coordinating motif, they exhibit distinct profiles for AF vs time. This difference can be attributed to the different nature and size of the water solubilizing moieties. The larger size PEG block which presents ethylene oxide units presents a stronger physical barrier against DTT penetration compared to the substantially smaller and more hydrophilic sulfobetaine groups.[22,27] Similar trends were measured for the DTT stability test using polymer and monomer-capped AuNP and AuNS dispersions (data not shown).

Mechanistic Considerations. Photoligation provides clear benefits for ligating gold nanocolloids with LA-R ligands compared to conventional incubation methods. We hereby discuss a few mechanistic concepts to explain our findings. It is widely accepted that coordination of thiols onto gold surfaces involves thiolate−Au complexation, the mechanism of which involves the interaction between (RS^-) and Au(I), due to electron transfer from the gold, followed by electrostatic binding.[90−92] More recently, studies by Reimers and co-workers have proposed that a better picture involves a transformation of thiol into thiyl (RS·), which interacts via electron transfer to Au(0), yielding the Au−S−R bond.[7,93,94] They further proposed based on DFT calculations that for

https://dx.doi.org/10.1021/acs.chemmater.0c02482
Chem. Mater. 2020, 32, 7469−7483

nanoparticles binding via thiyl−Au(0) formation is energetically more favorable than that involving thiolate−Au(I). This implies that in our case reduction of the dithiolane ring yielding thiol-containing products (e.g., dithiol) is required to promote ligand coordination on the gold nanocolloids. We thus stipulate that in the conventional incubation route ligand exchange with LA−R or disulfide−R molecules involves two steps, as proposed for SAM structures: physisorption of the disulfide molecules onto the gold surface, via attractive van der Waals forces, followed by chemisorption where homolytic cleavage of the S−S takes place.[38,90,92,95−101] In this scenario, schematically illustrated in Figure 7A, ligand substitution is slow. Experimentally, physisorption and bond-breaking events are inferred from studies showing that SAMs formed from either monothiol (HS−R) or disulfide (R−S−S−R′) molecules are indistinguishable.[42,90,97,101−103]

Photoligation has been successfully exploited to coat QDs and Au nanocrystals, and a few existing qualitative models have attempted to identify the rationale that make this route faster than incubation alone.[42,50−53,89,102,104] This strategy does not necessarily require initial physisorption, as viewed above, because UV-irradiation of free LA molecules has been shown to promote rapid photochemical transformation of the dithiolane rings to dithiyl, followed by several possible reaction pathways producing several thiol products including dihydrolipoic acid, polysulfide, sulfenic acid, and sulfoxide (Figure 7B,C).[51,53,105−108] Thus, coordination of the LA−R ligands occurs via two reaction steps: (i) a rapid photoinduced homolytic cleavage of S−S bond, which eliminates the requirement for initial adsorption and circumvents the activation energy required for S−S bond breaking in a typical binding reaction, and (ii) thiol−Au complexation, as schematically represented in Figure 7B. This scenario is energetically favorable based on reaction enthalpy considerations. More precisely, conventional coordination involves one endothermic S−S bond breaking, with $\Delta H \sim +30$ kcal/mol in a ring structure,[108] and formation of two thiol-to-Au bonds, an exothermic event with $\Delta H \sim -40$ kcal/mol per bond.[92,102] This would yield a net enthalpy of binding reaction, $\Delta H_{net/reaction} \sim -50$ kcal/mol. In comparison, the bond breaking term can be neglected in a photoligation process, and the total enthalpy required is $\Delta H_{Photo} \sim -80$ kcal/mol. This would imply that even though both binding reactions are spontaneous, photoligation is thermodynamically more favorable. These considerations would also imply that in a conventional coordination involving LA−R, binding would require accessing two adjacent sites on the gold nanosurfaces, while a single coordination site would be sufficient for chemisorption of LA*, since each sulfur in the dithiyl radical (or thiol in the dithiol group) can form one S−Au complex.[42,95,102] As a result, the competitive coordination of oxidized LAs onto Au nanocolloids is a slow process, whereas the abundance of dithiyl species under UV-irradiation leads to much faster ligand binding.

We further tested the validity of these mechanistic rationales by comparing the use of photoligation vs conventional incubation to coat oleylamine-coated AuNPs with LA or LA-ZW ligands in polar methanol or DMF (antisolvents for the native NPs). In this case, we found that conventional incubation of oleylamine−AuNPs (as aggregates) with these LA ligands is extremely slow, often yielding poor quality materials. This can be attributed to a reduced ligand adsorption/chemisorption rate per AuNP due to shielding of NP surfaces in the close-packed aggregates.[42] In comparison, the higher reactivity of LA* species enables rapid chemisorption, first by complexing with accessible NPs followed by further complexation with those deeply buried within the pellet. Given the spontaneity of these interactions, rapid "dissolution" of the pellet takes place under these conditions leading to the formation of homogeneous dispersions of NPs. Such a conclusion is supported by the data shown in Figure 1D, where UV-irradiation promotes rapid dispersion of the AuNP pellets (within 10 min), followed by homogenization of the dispersion.[48,95]

Prior results indicate that though fission of the dithiolane rings is key, effectiveness of the photoligation strategy applied to QDs is better when the procedure is performed *in situ*.[51] We tested the validity of this assumption by carrying out two control reactions under *ex situ* conditions using prereduced LA ligands. In the first, oleylamine−AuNPs (dispersed in hexane) were reacted, in a two-phase configuration, with either DHLA-PEG ($NaBH_4$-reduced) or preirradiated LA-PEG* ligands in MeOH; excess ligand with respect to NPs was ≤120000. These conditions produced rapid macroscopic phase transfer from hexane to MeOH, but the resulting NPs were prone to aggregation during standard processing (see Table S2).[42] In the second, 30 min incubation of a two-phase solution made of oleylamine−AuNPs in hexane and either DHLA (chemically reduced) or LA* in methanol also yielded irreversible aggregation. However, this reaction is successful when performed by using *in situ* UV-irradiation starting with oxidized LAs (see above). This can be attributed to the ability of the thiyl groups to rapidly sample the Au colloid surfaces and promote complexation yielding Au−S bonded ligands.[7,93]

Finally, we tested whether or not the short-lived thiyl radicals, generated during photoligation, play any role in the photoligation by speeding up the ligand substitution and homogenization of the samples.[51,53,108] For this, two dispersions containing AuNPs mixed with lipoic acid in DMF: one was supplemented with 2,2,6,6-tetramethyl-1-piperidinyloxy (TEMPO, a stable radical scavenger), and the other was not. A molar ratio of TEMPO:LA ∼ 8 was used. The samples were UV-irradiated and periodically inspected and imaged for up to 60 min. Figure 7D shows two sets of white light images acquired for the samples during the *in situ* irradiation. Data show that in the sample of the AuNP-plus-ligand mixture without TEMPO the NP aggregates experienced a fast homogenization within ∼8 min (see left set). In comparison, the right set shows the evolution of the same reaction in the presence of TEMPO, where ligand homogenization was slower, requiring up to ∼1 h. We also found that adding larger excess TEMPO could not completely quench the ligand exchange process, as homogenization eventually occurred after longer irradiation time. We attribute this result to the short lifetime of the radicals ($\tau \sim 75$ ns at room temperature),[105,108] where a fraction of those initially generated can rapidly convert to sulfhydryl by abstracting protons from protic molecules in the solution.[53] We conclude based on this result that *in situ* photoligation could facilitate the capture of dithiyl radicals (before they are transformed to other species) by gold surface atoms via a process that is energetically more favorable and does not necessarily involve thiolate−Au(I) formation, as suggested by Reimers and coworkers.[7,93,94] This model results in coordination interactions that are rapid and with increased effectiveness. These *in situ* interactions enhance the efficiency of ligand substitution

https://dx.doi.org/10.1021/acs.chemmater.0c02482
Chem. Mater. 2020, 32, 7469−7483

process while requiring smaller excess of ligands compared to conventional incubation.[51,53,104,109] Finally, the rationales discussed above regarding the fast chemisorption and energetically more favorable ligand−Au complexation achieved by using photoligation can also explain our recent observation, where LA−R* ligands were shown to competitively displace AuNP-bound mCherry−His fluorescent proteins at lower ligand concentration compared to their oxidized counterparts.[56]

CONCLUSION

We have shown that photoligation of various gold colloids with several lipoic acid-based ligands provides a simple and highly effective strategy for promoting *in situ* rapid ligand exchange, allowing the dispersion and manipulation of such materials under varying conditions. This strategy relies on the incubation of gold nanostructures with the oxidized form of the ligands, under UV-irradiation, and takes advantage of the photosensitive nature the ligands to a flux that overlaps with its absorption band centered at 335 nm. Such irradiation promotes the photochemical transformation of the dithiolane rings and yields highly reactive compounds (presenting dithyl radicals and thiol-modified products) that rapidly displace the native coating and chemisorb on the gold surfaces. It can be completed within ∼30 min, while consuming ∼10-fold less ligands compared to conventional incubation (without of photoirradiation). The resulting materials were characterized by using several analytical techniques, including optical absorption, TEM, DLS, FT-IR, and solution phase ^{1}H NMR spectroscopy, all of which proved that complete substitution of the native ligands (e.g., oleylamine, CTAB, PVP, and citrate) with LA-R ligands has taken place. This strategy provides homogeneous and aggregate-free gold nanocolloid dispersions that exhibit long-term colloidal stability over a broad range of biologically relevant conditions, while preserving the structural and photophysical properties of the nanocolloids intact.

The strategy can be applied to any LA-containing ligand regardless of its structure (monomers, polymers, or mixed coordination) and whether or not it presents reactive groups (e.g., −COOH, $-NH_2$, $-N_3$, and −CHO). This makes the ligand exchange method suitable for preparing plasmonic gold platforms that exhibit controllable and specific reactivity, readily adapted for easy interfacing with biology. The photoligation route is potentially applicable to other metallic single or mixed metal core nanocolloids (Ag and Ag-containing nanostructures), making it potentially very promising for designing multifunctional nanoscale platforms with application in sensor design, Raman scattering, and energy transfer interactions.

EXPERIMENTAL SECTION

Growth of PVP-Coated Gold Nanostars, PVP-AuNSs. PVP-AuNSs ($d \times l$ = 25 nm × 12 nm, TEM data) were synthesized following the protocol originally reported Liz-Marzán and co-workers, with a slight few modifications.[70] The starting spherical gold seeds were prepared via $NaBH_4$ reduction of $HAuCl_4$ in the presence of polyvinylpyrrolidone (PVP, M_w 10000 Da). Briefly, in a 100 mL one-neck round-bottom flask equipped with a stir bar, 0.017 g of PVP was dissolved in a mixture of DMF (45 mL) and DI water (2.5 mL). A 22 μL aliquot of 0.1136 M gold solution was then added under vigorous stirring. Next, 2.5 mL of 10 mM freshly prepared $NaBH_4$ solution was rapidly injected into the flask, and the reaction mixture was further stirred for another 2 h and then aged for 24 h, before use in the growth of nanostars. Growth solution was prepared as follows: in a 100 mL one-neck round-bottom flask, 108 μL of 0.1136 M gold precursor solution was added to 45 mL of 10 mM PVP solution in DMF under vigorous stirring. After 6 min, 102 μL of performed-seed dispersion (ratio of $[HAuCl_4]/[seed]$ = 2424) was added. The mixture changed color from faint yellow, to colorless, to slightly blue within 10 min, and eventually to dark blue after 40 min. We note that sedimentation of the colloids tends to build up after extended storage (∼2−3 weeks). However, applying sonication for few minutes or simple stirring would homogenize the sample. Protocols used for growing the other gold colloids (namely, Au nanorods and Au nanoparticles) are provided in the Supporting Information.

Ligand Exchange Promoted by UV-Irradiation (Photoligation). Photoligation of the various Au colloids with LA-based ligands was implemented using either one-phase reaction (one solvent) or two-phase reaction (using two immiscible solvents). However, there are few instances where the two-phase route is required, in particular when the starting materials and ligands cannot be dispersed in the same solvent (e.g., oleylamine-AuNPs and LA-ZW). We briefly describe the protocols for both routes. Additional details are provided in the Supporting Information.

One-Phase Reaction. We will refer to this reaction condition as "homogeneous photoligation". It has been applied to cap exchange citrate-AuNPs and CTAB-AuNRs with LA-based ligands in basic aqueous conditions (e.g., phosphate buffer, pH 7.6); photoligation of PVP-AuNSs with LA-R ligands in methanol; and photoligation of oleylamine−AuNPs with LA-PIMA-PEG in $CHCl_3$. We describe the procedure applied to ligate PVP-AuNSs with LA-ZW. Briefly, 3 mL of a PVP-AuNSs stock dispersion (0.51 nM) was centrifuged at 10000 rpm for 10 min. The supernatant was discarded, and the pellet was redispersed in 200 μL of MeOH, followed by transfer into a scintillation vial equipped with a stir bar. Separately, a ligand solution was prepared by dissolving 0.8 mg of LA-ZW in 400 μL of MeOH and heating it at 60 °C for 2−3 h (using a water bath). The ligand solution was mixed with the AuNS dispersion and then placed inside the UV reactor and irradiated for 30 min while stirring; the used conditions provide a molar ratio of LA-ZW to AuNSs = 1200000. The macroscopic aggregates of gold colloids formed during irradiation were isolated from the yellowish supernatant by centrifugation at 3500 rpm for 2 min. The precipitate was dried under air flow then dispersed in 4 mL of DI water. The dispersion was passed through a syringe filter (0.45 μm, PTFE) and further purified from excess ligands and other solubilized precursors/impurities by applying 3−4 rounds of concentration/dilution using a membrane filtration device (Millipore, M_w cutoff = 100000 Da). The dispersion was transferred to a clean scintillation vial and stored at 4 °C until further use. The protocols for photoligating PVP-AuNSs with other LA-based ligands, CTAB-AuNRs, and citrate-AuNPs with LA-based ligands are provided in the Supporting Information.

Two-Phase Reaction. We refer to this reaction condition as "heterogeneous photoligation", as the ligand exchange is accompanied by phase transfer. We summarize the photoligation of oleylamine−AuNPs with LA-ZW. A 50 μL aliquot of oleylamine−AuNPs in hexane (from a stock dispersion, 0.37 μM) was diluted with 400 μL of hexane by using a scintillation vial equipped with a stir bar. Separately, 0.92 mg of LA-ZW was dissolved in 300 μL of MeOH containing ∼1 mg of TMAH and slightly heated at 60 °C by using a water bath (for 2−3 h). The ligand solution was slowly added to the colloid dispersion, followed by few drops (∼30−50 μL) of $CHCl_3$. The vial was placed in the UV reactor and irradiated for 30 min. This yields AuNP precipitates, which is an early indication of ligand substitution. The precipitates were centrifuged at 3500 rpm for 2 min, and then the supernatant was discarded by using a pipet, followed by hexane wash (500 μL) and drying under nitrogen flow. DI water (∼1−2 mL) was added to the dried pellet of LA-ZW-AuNPs, yielding a reddish dispersion, which was passed through a syringe filter (0.45 μm, PTFE) and further purified by applying 2−3 rounds of concentration/dilution with DI water using a membrane filtration device (Millipore, M_w cutoff = 100000 Da), as above, and then stored at 4 °C. The two-phase photoligation of oleylamine−AuNP with LA-PEG or LA ligands is provided in the Supporting Information.

https://dx.doi.org/10.1021/acs.chemmater.0c02482
Chem. Mater. 2020, 32, 7469−7483

■ ASSOCIATED CONTENT

Supporting Information

The Supporting Information is available free of charge at https://pubs.acs.org/doi/10.1021/acs.chemmater.0c02482.

Detailed information about materials, instrumentation, additional details on the ligand synthesis, nanoparticles synthesis, photoligation reactions, conditions of colloidal stability tests, DLS background and DLS data of oleylamine- and citrate-stabilized AuNPs, PL data of PVP-AuNSs, and an estimate of surface area of gold nanostructures (PDF)

■ AUTHOR INFORMATION

Corresponding Author

Hedi Mattoussi − *Department of Chemistry and Biochemistry, Florida State University, Tallahassee, Florida 32306, United States;* orcid.org/0000-0002-6511-9323; Email: mattoussi@fsu.edu

Authors

Zhicheng Jin − *Department of Chemistry and Biochemistry, Florida State University, Tallahassee, Florida 32306, United States*

Yuya Sugiyama − *Department of Chemistry and Biochemistry, Florida State University, Tallahassee, Florida 32306, United States; Asahi Kasei Corporation, Fuji City, Shizuoka 416-8501, Japan*

Chengqi Zhang − *Department of Chemistry and Biochemistry, Florida State University, Tallahassee, Florida 32306, United States; Genista Biosciences, San Jose, California 95138, United States*

Goutam Palui − *Department of Chemistry and Biochemistry, Florida State University, Tallahassee, Florida 32306, United States; National Center for Toxicological Research, The Food and Drug Administration, Jefferson, Arkansas 72079, United States*

Yan Xin − *National High Magnetic Field Laboratory, Florida State University, Tallahassee, Florida 32310, United States*

Liang Du − *Department of Chemistry and Biochemistry, Florida State University, Tallahassee, Florida 32306, United States*

Sisi Wang − *Department of Chemistry and Biochemistry, Florida State University, Tallahassee, Florida 32306, United States*

Narjes Dridi − *Department of Chemistry and Biochemistry, Florida State University, Tallahassee, Florida 32306, United States*

Complete contact information is available at: https://pubs.acs.org/10.1021/acs.chemmater.0c02482

Notes

The authors declare no competing financial interest.

■ ACKNOWLEDGMENTS

We thank FSU (NSF-CHE # 1508501), the National Institutes of Health (NIH # R01 DC013080), AFOSR (Grant #FA9550-18-1-0144), and Asahi-Kasei Corp. for financial support. The TEM work was performed at the FSU TEM facility, supported by the Florida State University Research Foundation, the National High Magnetic Field Laboratory (DMR-1644779), and the State of Florida. We also thank Susan Hellstrom for the fruitful discussions.

■ REFERENCES

(1) Daniel, M. C.; Astruc, D. Gold nanoparticles: Assembly, supramolecular chemistry, quantum-size-related properties, and applications toward biology, catalysis, and nanotechnology. *Chem. Rev.* **2004**, *104*, 293−346.

(2) Lee, S.; Cha, E.-J.; Park, K.; Lee, S.-Y.; Hong, J.-K.; Sun, I.-C.; Kim, S. Y.; Choi, K.; Kwon, I. C.; Kim, K.; Ahn, C.-H. A Near-Infrared-Fluorescence-Quenched Gold-Nanoparticle Imaging Probe for In Vivo Drug Screening and Protease Activity Determination. *Angew. Chem., Int. Ed.* **2008**, *47*, 2804−2807.

(3) von Maltzahn, G.; Park, J.-H.; Agrawal, A.; Bandaru, N. K.; Das, S. K.; Sailor, M. J.; Bhatia, S. N. Computationally Guided Photothermal Tumor Therapy Using Long-Circulating Gold Nanorod Antennas. *Cancer Res.* **2009**, *69*, 3892−3900.

(4) Dreaden, E. C.; Alkilany, A. M.; Huang, X.; Murphy, C. J.; El-Sayed, M. A. The golden age: gold nanoparticles for biomedicine. *Chem. Soc. Rev.* **2012**, *41*, 2740−2779.

(5) Giner-Casares, J. J.; Henriksen-Lacey, M.; Coronado-Puchau, M.; Liz-Marzán, L. M. Inorganic nanoparticles for biomedicine: where materials scientists meet medical research. *Mater. Today* **2016**, *19*, 19−28.

(6) Burrows, N. D.; Lin, W.; Hinman, J. G.; Dennison, J. M.; Vartanian, A. M.; Abadeer, N. S.; Grzincic, E. M.; Jacob, L. M.; Li, J.; Murphy, C. J. Surface Chemistry of Gold Nanorods. *Langmuir* **2016**, *32*, 9905−9921.

(7) Reimers, J. R.; Ford, M. J.; Marcuccio, S. M.; Ulstrup, J.; Hush, N. S. Competition of van der Waals and chemical forces on gold−sulfur surfaces and nanoparticles. *Nat. Rev. Chem.* **2017**, *1*, 0017.

(8) Falagan-Lotsch, P.; Grzincic, E. M.; Murphy, C. J. New Advances in Nanotechnology-Based Diagnosis and Therapeutics for Breast Cancer: An Assessment of Active-Targeting Inorganic Nanoplatforms. *Bioconjugate Chem.* **2017**, *28*, 135−152.

(9) Polavarapu, L.; Perez-Juste, J.; Xu, Q.-H.; Liz-Marzan, L. M. Optical sensing of biological, chemical and ionic species through aggregation of plasmonic nanoparticles. *J. Mater. Chem. C* **2014**, *2*, 7460−7476.

(10) Langer, J.; Jimenez de Aberasturi, D.; Aizpurua, J.; Alvarez-Puebla, R. A.; Auguié, B.; Baumberg, J. J.; Bazan, G. C.; Bell, S. E. J.; Boisen, A.; Brolo, A. G.; et al. Present and Future of Surface-Enhanced Raman Scattering. *ACS Nano* **2020**, *14*, 28−117.

(11) Espinosa, A.; Silva, A. K. A.; Sánchez-Iglesias, A.; Grzelczak, M.; Péchoux, C.; Desboeufs, K.; Liz-Marzán, L. M.; Wilhelm, C. Cancer Cell Internalization of Gold Nanostars Impacts Their Photothermal Efficiency In Vitro and In Vivo: Toward a Plasmonic Thermal Fingerprint in Tumoral Environment. *Adv. Healthcare Mater.* **2016**, *5*, 1040−1048.

(12) Jiang, Y.; Huo, S.; Mizuhara, T.; Das, R.; Lee, Y.-W.; Hou, S.; Moyano, D. F.; Duncan, B.; Liang, X.-J.; Rotello, V. M. The Interplay of Size and Surface Functionality on the Cellular Uptake of Sub-10 nm Gold Nanoparticles. *ACS Nano* **2015**, *9*, 9986−9993.

(13) Howes, P. D.; Chandrawati, R.; Stevens, M. M. Colloidal nanoparticles as advanced biological sensors. *Science* **2014**, *346*, 1247390.

(14) Li, N.; Zhao, P.; Astruc, D. Anisotropic Gold Nanoparticles: Synthesis, Properties, Applications, and Toxicity. *Angew. Chem., Int. Ed.* **2014**, *53*, 1756−1789.

(15) Chinen, A. B.; Guan, C. M.; Ferrer, J. R.; Barnaby, S. N.; Merkel, T. J.; Mirkin, C. A. Nanoparticle Probes for the Detection of Cancer Biomarkers, Cells, and Tissues by Fluorescence. *Chem. Rev.* **2015**, *115*, 10530−10574.

(16) Near, R. D.; Hayden, S. C.; Hunter, R. E.; Thackston, D.; El-Sayed, M. A. Rapid and Efficient Prediction of Optical Extinction Coefficients for Gold Nanospheres and Gold Nanorods. *J. Phys. Chem. C* **2013**, *117*, 23950−23955.

(17) de Puig, H.; Tam, J. O.; Yen, C.-W.; Gehrke, L.; Hamad-Schifferli, K. Extinction Coefficient of Gold Nanostars. *J. Phys. Chem. C* **2015**, *119*, 17408−17415.

(18) Liu, X.; Atwater, M.; Wang, J.; Huo, Q. Extinction coefficient of gold nanoparticles with different sizes and different capping ligands. *Colloids Surf., B* **2007**, *58*, 3−7.
(19) Huang, X.; Neretina, S.; El-Sayed, M. A. Gold Nanorods: From Synthesis and Properties to Biological and Biomedical Applications. *Adv. Mater.* **2009**, *21*, 4880−4910.
(20) Zhan, N.; Palui, G.; Kapur, A.; Palomo, V.; Dawson, P. E.; Mattoussi, H. Controlling the Architecture, Coordination, and Reactivity of Nanoparticle Coating Utilizing an Amino Acid Central Scaffold. *J. Am. Chem. Soc.* **2015**, *137*, 16084−16097.
(21) Lin, C. A.; Sperling, R. A.; Li, J. K.; Yang, T. Y.; Li, P. Y.; Zanella, M.; Chang, W. H.; Parak, W. J. Design of an amphiphilic polymer for nanoparticle coating and functionalization. *Small* **2008**, *4*, 334−341.
(22) Hostetler, M. J.; Templeton, A. C.; Murray, R. W. Dynamics of Place-Exchange Reactions on Monolayer-Protected Gold Cluster Molecules. *Langmuir* **1999**, *15*, 3782−3789.
(23) Kang, Y. J.; Taton, T. A. Core/shell gold nanoparticles by self-assembly and crosslinking of micellar, block-copolymer shells. *Angew. Chem., Int. Ed.* **2005**, *44*, 409−412.
(24) Ducongé, F.; Pons, T.; Pestourie, C.; Hérin, L.; Thézé, B.; Gombert, K.; Mahler, B.; Hinnen, F.; Kühnast, B.; Dollé, F.; Dubertret, B.; Tavitian, B. Fluorine-18-Labeled Phospholipid Quantum Dot Micelles for in Vivo Multimodal Imaging from Whole Body to Cellular Scales. *Bioconjugate Chem.* **2008**, *19*, 1921−1926.
(25) Yu, W. W.; Chang, E.; Falkner, J. C.; Zhang, J. Y.; Al-Somali, A. M.; Sayes, C. M.; Johns, J.; Drezek, R.; Colvin, V. L. Forming biocompatible and nonaggregated nanocrystals in water using amphiphilic polymers. *J. Am. Chem. Soc.* **2007**, *129*, 2871−2879.
(26) Du, L.; Wang, W.; Zhang, C.; Jin, Z.; Palui, G.; Mattoussi, H. A Versatile Coordinating Ligand for Coating Semiconductor, Metal, and Metal Oxide Nanocrystals. *Chem. Mater.* **2018**, *30*, 7269−7279.
(27) Wang, W.; Ji, X.; Du, L.; Mattoussi, H. Enhanced Colloidal Stability of Various Gold Nanostructures Using a Multicoordinating Polymer Coating. *J. Phys. Chem. C* **2017**, *121*, 22901−22913.
(28) Mei, B. C.; Oh, E.; Susumu, K.; Farrell, D.; Mountziaris, T. J.; Mattoussi, H. Effects of Ligand Coordination Number and Surface Curvature on the Stability of Gold Nanoparticles in Aqueous Solutions. *Langmuir* **2009**, *25*, 10604−10611.
(29) Dubertret, B.; Skourides, P.; Norris, D. J.; Noireaux, V.; Brivanlou, A. H.; Libchaber, A. In vivo imaging of quantum dots encapsulated in phospholipid micelles. *Science* **2002**, *298*, 1759−1762.
(30) Kang, J. S.; Taton, T. A. Oligothiol Graft-Copolymer Coatings Stabilize Gold Nanoparticles against Harsh Experimental Conditions. *Langmuir* **2012**, *28*, 16751−16760.
(31) Lin, C. A. J.; Sperling, R. A.; Li, J. K.; Yang, T. Y.; Li, P. Y.; Zanella, M.; Chang, W. H.; Parak, W. G. J. Design of an amphiphilic polymer for nanoparticle coating and functionalization. *Small* **2008**, *4*, 334−341.
(32) Pearson, R. G. Hard and Soft Acids and Bases. *J. Am. Chem. Soc.* **1963**, *85*, 3533−3539.
(33) Zhong, J.; Qu, J.; Ye, F.; Wang, C.; Meng, L.; Yang, J. The bis(p-sulfonatophenyl)phenylphosphine-assisted synthesis and phase transfer of ultrafine gold nanoclusters. *J. Colloid Interface Sci.* **2011**, *361*, 59−63.
(34) Rouhana, L. L.; Jaber, J. A.; Schlenoff, J. B. Aggregation-Resistant Water-Soluble Gold Nanoparticles. *Langmuir* **2007**, *23*, 12799−12801.
(35) Oh, E.; Susumu, K.; Mäkinen, A. J.; Deschamps, J. R.; Huston, A. L.; Medintz, I. L. Colloidal Stability of Gold Nanoparticles Coated with Multithiol-Poly(ethylene glycol) Ligands: Importance of Structural Constraints of the Sulfur Anchoring Groups. *J. Phys. Chem. C* **2013**, *117*, 18947−18956.
(36) Mei, B. C.; Susumu, K.; Medintz, I. L.; Delehanty, J. B.; Mountziaris, T. J.; Mattoussi, H. Modular poly(ethylene glycol) ligands for biocompatible semiconductor and gold nanocrystals with extended pH and ionic stability. *J. Mater. Chem.* **2008**, *18*, 4949−4958.
(37) Nuzzo, R. G.; Allara, D. L. Adsorption of bifunctional organic disulfides on gold surfaces. *J. Am. Chem. Soc.* **1983**, *105*, 4481−4483.
(38) Vericat, C.; Vela, M. E.; Benitez, G.; Carro, P.; Salvarezza, R. C. Self-assembled monolayers of thiols and dithiols on gold: new challenges for a well-known system. *Chem. Soc. Rev.* **2010**, *39*, 1805−1834.
(39) Dinkel, R.; Braunschweig, B.; Peukert, W. Fast and Slow Ligand Exchange at the Surface of Colloidal Gold Nanoparticles. *J. Phys. Chem. C* **2016**, *120*, 1673−1682.
(40) Navarro, J. R G.; Manchon, D.; Lerouge, F.; Blanchard, N. P.; Marotte, S.; Leverrier, Y.; Marvel, J.; Chaput, F.; Micouin, G.; Gabudean, A.-M.; Mosset, A.; Cottancin, E.; Baldeck, P. L.; Kamada, K.; Parola, S. Synthesis of PEGylated gold nanostars and bipyramids for intracellular uptake. *Nanotechnology* **2012**, *23*, 465602.
(41) Smith, A. M.; Marbella, L. E.; Johnston, K. A.; Hartmann, M. J.; Crawford, S. E.; Kozycz, L. M.; Seferos, D. S.; Millstone, J. E. Quantitative Analysis of Thiolated Ligand Exchange on Gold Nanoparticles Monitored by 1H NMR Spectroscopy. *Anal. Chem.* **2015**, *87*, 2771−2778.
(42) Ma, Y.; Chechik, V. Aging of Gold Nanoparticles: Ligand Exchange with Disulfides. *Langmuir* **2011**, *27*, 14432−14437.
(43) Wang, W.; Ji, X.; Burns, H.; Mattoussi, H. A multi-coordinating polymer ligand optimized for the functionalization of metallic nanocrystals and nanorods. *Faraday Discuss.* **2016**, *191*, 481−494.
(44) Park, C. S.; Lee, H. J.; Jamison, A. C.; Lee, T. R. Robust Maleimide-Functionalized Gold Surfaces and Nanoparticles Generated Using Custom-Designed Bidentate Adsorbates. *Langmuir* **2016**, *32*, 7306−7315.
(45) Sahu, P.; Shimpi, J.; Lee, H. J.; Lee, T. R.; Prasad, B. L. V. Digestive Ripening of Au Nanoparticles Using Multidentate Ligands. *Langmuir* **2017**, *33*, 1943−1950.
(46) Marquez, M. D.; Zenasni, O.; Jamison, A. C.; Lee, T. R. Homogeneously Mixed Monolayers: Emergence of Compositionally Conflicted Interfaces. *Langmuir* **2017**, *33*, 8839−8855.
(47) Liu, B.; Liu, J. Freezing Directed Construction of Bio/Nano Interfaces: Reagentless Conjugation, Denser Spherical Nucleic Acids, and Better Nanoflares. *J. Am. Chem. Soc.* **2017**, *139*, 9471−9474.
(48) Khan, M. N.; Zharnikov, M. Irradiation Promoted Exchange Reaction with Disulfide Substituents. *J. Phys. Chem. C* **2013**, *117*, 14534−14543.
(49) Sahli, R.; Fave, C.; Raouafi, N.; Boujlel, K.; Schöllhorn, B.; Limoges, B. Switching On/Off the Chemisorption of Thioctic-Based Self-Assembled Monolayers on Gold by Applying a Moderate Cathodic/Anodic Potential. *Langmuir* **2013**, *29*, 5360−5368.
(50) Palui, G.; Avellini, T.; Zhan, N.; Pan, F.; Gray, D.; Alabugin, I.; Mattoussi, H. Photoinduced Phase Transfer of Luminescent Quantum Dots to Polar and Aqueous Media. *J. Am. Chem. Soc.* **2012**, *134*, 16370−16378.
(51) Aldeek, F.; Hawkins, D.; Palomo, V.; Safi, M.; Palui, G.; Dawson, P. E.; Alabugin, I.; Mattoussi, H. UV and Sunlight Driven Photoligation of Quantum Dots: Understanding the Photochemical Transformation of the Ligands. *J. Am. Chem. Soc.* **2015**, *137*, 2704−2714.
(52) ten Hove, J. B.; Schijven, L. M. I.; Wang, J.; Velders, A. H. Size-controlled and water-soluble gold nanoparticles using UV-induced ligand exchange and phase transfer. *Chem. Commun.* **2018**, *54*, 13355−13358.
(53) Mishra, D.; Wang, S.; Michel, S.; Palui, G.; Zhan, N.; Perng, W.; Jin, Z.; Mattoussi, H. Photochemical transformation of lipoic acid-based ligands: probing the effects of solvent, ligand structure, oxygen and pH. *Phys. Chem. Chem. Phys.* **2018**, *20*, 3895−3902.
(54) Wang, W.; Kapur, A.; Ji, X.; Safi, M.; Palui, G.; Palomo, V.; Dawson, P. E.; Mattoussi, H. Photoligation of an Amphiphilic Polymer with Mixed Coordination Provides Compact and Reactive Quantum Dots. *J. Am. Chem. Soc.* **2015**, *137*, 5438−5451.
(55) Moroz, P.; Jin, Z.; Sugiyama, Y.; Lara, D. A.; Razgoniaeva, N.; Yang, M.; Kholmicheva, N.; Khon, D.; Mattoussi, H.; Zamkov, M. Competition of Charge and Energy Transfer Processes in Donor−

https://dx.doi.org/10.1021/acs.chemmater.0c02482
Chem. Mater. 2020, 32, 7469−7483

Acceptor Fluorescence Pairs: Calibrating the Spectroscopic Ruler. *ACS Nano* **2018**, *12*, 5657−5665.
(56) Kapur, A.; Aldeek, F.; Ji, X.; Safi, M.; Wang, W.; Del Cid, A.; Steinbock, O.; Mattoussi, H. Self-Assembled Gold Nanoparticle−Fluorescent Protein Conjugates as Platforms for Sensing Thiolate Compounds via Modulation of Energy Transfer Quenching. *Bioconjugate Chem.* **2017**, *28*, 678−687.
(57) Hiramatsu, H.; Osterloh, F. E. A Simple Large-Scale Synthesis of Nearly Monodisperse Gold and Silver Nanoparticles with Adjustable Sizes and with Exchangeable Surfactants. *Chem. Mater.* **2004**, *16*, 2509−2511.
(58) Liu, S.; Chen, G.; Prasad, P. N.; Swihart, M. T. Synthesis of Monodisperse Au, Ag, and Au−Ag Alloy Nanoparticles with Tunable Size and Surface Plasmon Resonance Frequency. *Chem. Mater.* **2011**, *23*, 4098−4101.
(59) Aldeek, F.; Safi, M.; Zhan, N. Q.; Palui, G.; Mattoussi, H. Understanding the Self-Assembly of Proteins onto Gold Nanoparticles and Quantum Dots Driven by Metal-Histidine Coordination. *ACS Nano* **2013**, *7*, 10197−10210.
(60) Tournebize, J.; Boudier, A.; Sapin-Minet, A.; Maincent, P.; Leroy, P.; Schneider, R. Role of Gold Nanoparticles Capping Density on Stability and Surface Reactivity to Design Drug Delivery Platforms. *ACS Appl. Mater. Interfaces* **2012**, *4*, 5790−5799.
(61) Brown, K. R.; Walter, D. G.; Natan, M. J. Seeding of Colloidal Au Nanoparticle Solutions. 2. Improved Control of Particle Size and Shape. *Chem. Mater.* **2000**, *12*, 306−313.
(62) Ji, X.; Song, X.; Li, J.; Bai, Y.; Yang, W.; Peng, X. Size Control of Gold Nanocrystals in Citrate Reduction: The Third Role of Citrate. *J. Am. Chem. Soc.* **2007**, *129*, 13939−13948.
(63) Turkevich, J.; Stevenson, P. C.; Hillier, J. A Study of the Nucleation and Growth Processes in the Synthesis of Colloidal Gold. *Discuss. Faraday Soc.* **1951**, *11*, 55.
(64) Enustun, B. V.; Turkevich, J. Coagulation of Colloidal Gold. *J. Am. Chem. Soc.* **1963**, *85*, 3317−3328.
(65) Yang, M.; Moroz, P.; Jin, Z.; Budkina, D. S.; Sundrani, N.; Porotnikov, D.; Cassidy, J.; Sugiyama, Y.; Tarnovsky, A. N.; Mattoussi, H.; Zamkov, M. Delayed Photoluminescence in Metal-Conjugated Fluorophores. *J. Am. Chem. Soc.* **2019**, *141*, 11286−11297.
(66) Jana, N. R.; Gearheart, L.; Murphy, C. J. Wet Chemical Synthesis of High Aspect Ratio Cylindrical Gold Nanorods. *J. Phys. Chem. B* **2001**, *105*, 4065−4067.
(67) Sau, T. K.; Murphy, C. J. Room temperature, high-yield synthesis of multiple shapes of gold nanoparticles in aqueous solution. *J. Am. Chem. Soc.* **2004**, *126*, 8648−8649.
(68) Ye, X.; Jin, L.; Caglayan, H.; Chen, J.; Xing, G.; Zheng, C.; Doan-Nguyen, V.; Kang, Y.; Engheta, N.; Kagan, C. R.; Murray, C. B. Improved Size-Tunable Synthesis of Monodisperse Gold Nanorods through the Use of Aromatic Additives. *ACS Nano* **2012**, *6*, 2804−2817.
(69) Ye, X.; Zheng, C.; Chen, J.; Gao, Y.; Murray, C. B. Using Binary Surfactant Mixtures To Simultaneously Improve the Dimensional Tunability and Monodispersity in the Seeded Growth of Gold Nanorods. *Nano Lett.* **2013**, *13*, 765−771.
(70) Barbosa, S.; Agrawal, A.; Rodríguez-Lorenzo, L.; Pastoriza-Santos, I.; Alvarez-Puebla, R. A.; Kornowski, A.; Weller, H.; Liz-Marzán, L. M. Tuning Size and Sensing Properties in Colloidal Gold Nanostars. *Langmuir* **2010**, *26*, 14943−14950.
(71) Zhan, N.; Palui, G.; Mattoussi, H. Preparation of compact biocompatible quantum dots using multicoordinating molecular-scale ligands based on a zwitterionic hydrophilic motif and lipoic acid anchors. *Nat. Protoc.* **2015**, *10*, 859−874.
(72) Mei, B. C.; Susumu, K.; Medintz, I. L.; Mattoussi, H. Polyethylene glycol-based bidentate ligands to enhance quantum dot and gold nanoparticle stability in biological media. *Nat. Protoc.* **2009**, *4*, 412−423.
(73) Jin, Z.; Du, L.; Zhang, C.; Sugiyama, Y.; Wang, W.; Palui, G.; Wang, S.; Mattoussi, H. Modification of Poly(maleic anhydride)-Based Polymers with H2N−R Nucleophiles: Addition or Substitution Reaction? *Bioconjugate Chem.* **2019**, *30*, 871−880.
(74) Gole, A.; Murphy, C. J. Polyelectrolyte-Coated Gold Nanorods: Synthesis, Characterization and Immobilization. *Chem. Mater.* **2005**, *17*, 1325−1330.
(75) Mehtala, J. G.; Zemlyanov, D. Y.; Max, J. P.; Kadasala, N.; Zhao, S.; Wei, A. Citrate-Stabilized Gold Nanorods. *Langmuir* **2014**, *30*, 13727−13730.
(76) SoRelle, E. D.; Liba, O.; Hussain, Z.; Gambhir, M.; de la Zerda, A. Biofunctionalization of Large Gold Nanorods Realizes Ultrahigh-Sensitivity Optical Imaging Agents. *Langmuir* **2015**, *31*, 12339−12347.
(77) Berne, B. J.; Pecora, R. *Dynamic Light Scattering: With Applications to Chemistry, Biology, and Physics*; Dover Publications: Mineola, NY, 2000.
(78) Hens, Z.; Martins, J. C. A Solution NMR Toolbox for Characterizing the Surface Chemistry of Colloidal Nanocrystals. *Chem. Mater.* **2013**, *25*, 1211−1221.
(79) De Nolf, K.; Cosseddu, S. M.; Jasieniak, J. J.; Drijvers, E.; Martins, J. C.; Infante, I.; Hens, Z. Binding and Packing in Two-Component Colloidal Quantum Dot Ligand Shells: Linear versus Branched Carboxylates. *J. Am. Chem. Soc.* **2017**, *139*, 3456−3464.
(80) Wu, M.; Vartanian, A. M.; Chong, G.; Pandiakumar, A. K.; Hamers, R. J.; Hernandez, R.; Murphy, C. J. Solution NMR Analysis of Ligand Environment in Quaternary Ammonium-Terminated Self-Assembled Monolayers on Gold Nanoparticles: The Effect of Surface Curvature and Ligand Structure. *J. Am. Chem. Soc.* **2019**, *141*, 4316−4327.
(81) Zeng, B.; Palui, G.; Zhang, C.; Zhan, N.; Wang, W.; Ji, X.; Chen, B.; Mattoussi, H. Characterization of the Ligand Capping of Hydrophobic CdSe−ZnS Quantum Dots Using NMR Spectroscopy. *Chem. Mater.* **2018**, *30*, 225−238.
(82) Van Lokeren, L.; Maheut, G.; Ribot, F.; Escax, V.; Verbruggen, I.; Sanchez, C.; Martins, J. C.; Biesemans, M.; Willem, R. Characterization of Titanium Dioxide Nanoparticles Dispersed in Organic Ligand Solutions by Using a Diffusion-Ordered Spectroscopy-Based Strategy. *Chem. - Eur. J.* **2007**, *13*, 6957−6966.
(83) Zhang, C.; Jin, Z.; Zeng, B.; Wang, W.; Palui, G.; Mattoussi, H. Characterizing the Brownian Diffusion of Nanocolloids and Molecular Solutions: Diffusion-Ordered NMR Spectroscopy vs Dynamic Light Scattering. *J. Phys. Chem. B* **2020**, *124*, 4631−4650.
(84) Zhang, C.; Palui, G.; Zeng, B.; Zhan, N.; Chen, B.; Mattoussi, H. Non-Invasive Characterization of the Organic Coating of Biocompatible Quantum Dots Using Nuclear Magnetic Resonance Spectroscopy. *Chem. Mater.* **2018**, *30*, 3454−3466.
(85) Kedia, A.; Senthil Kumar, P. Precursor-Driven Nucleation and Growth Kinetics of Gold Nanostars. *J. Phys. Chem. C* **2012**, *116*, 1679−1686.
(86) Song, G.; Lin, Y.; Zhu, Z.; Zheng, H.; Qiao, J.; He, C.; Wang, H. Strong Fluorescence of Poly(N-vinylpyrrolidone) and Its Oxidized Hydrolyzate. *Macromol. Rapid Commun.* **2015**, *36*, 278−285.
(87) Love, C. S.; Ashworth, I.; Brennan, C.; Chechik, V.; Smith, D. K. Dendron-protected Au nanoparticles—Effect of dendritic structure on chemical stability. *J. Colloid Interface Sci.* **2006**, *302*, 178−186.
(88) Weisbecker, C. S.; Merritt, M. V.; Whitesides, G. M. Molecular Self-Assembly of Aliphatic Thiols on Gold Colloids. *Langmuir* **1996**, *12*, 3763−3772.
(89) Jin, Z.; Kapur, A.; Wang, W.; Hernandez, J. D.; Thakur, M.; Mattoussi, H. The dual−function of lipoic acid groups as surface anchors and sulfhydryl reactive sites on polymer-stabilized QDs and Au nanocolloids. *J. Chem. Phys.* **2019**, *151*, 164703.
(90) Grönbeck, H.; Curioni, A.; Andreoni, W. Thiols and Disulfides on the Au(111) Surface: The Headgroup-Gold Interaction. *J. Am. Chem. Soc.* **2000**, *122*, 3839−3842.
(91) Xue, Y.; Li, X.; Li, H.; Zhang, W. Quantifying thiol−gold interactions towards the efficient strength control. *Nat. Commun.* **2014**, *5*, 4348.
(92) Schessler, H. M.; Karpovich, D. S.; Blanchard, G. J. Quantitating the Balance between Enthalpic and Entropic Forces in

Alkanethiol/Gold Monolayer Self Assembly. *J. Am. Chem. Soc.* **1996**, *118*, 9645−9651.
(93) Reimers, J. R.; Ford, M. J.; Halder, A.; Ulstrup, J.; Hush, N. S. Gold surfaces and nanoparticles are protected by Au(0)−thiyl species and are destroyed when Au(I)−thiolates form. *Proc. Natl. Acad. Sci. U. S. A.* **2016**, *113*, E1424−E1433.
(94) Reimers, J. R.; Wang, Y.; Cankurtaran, B. O.; Ford, M. J. Chemical Analysis of the Superatom Model for Sulfur-Stabilized Gold Nanoparticles. *J. Am. Chem. Soc.* **2010**, *132*, 8378−8384.
(95) Torrelles, X.; Vericat, C.; Vela, M. E.; Fonticelli, M. H.; Daza Millone, M. A.; Felici, R.; Lee, T.-L.; Zegenhagen, J.; Muñoz, G.; Martín-Gago, J. A.; Salvarezza, R. C. Two-Site Adsorption Model for the $(\sqrt{3} \times \sqrt{3})$-R30° Dodecanethiolate Lattice on Au(111) Surfaces. *J. Phys. Chem. B* **2006**, *110*, 5586−5594.
(96) Maksymovych, P.; Sorescu, D. C.; Yates, J. T. Gold-Adatom-Mediated Bonding in Self-Assembled Short-Chain Alkanethiolate Species on the Au(111) Surface. *Phys. Rev. Lett.* **2006**, *97*, 146103.
(97) Biebuyck, H. A.; Bain, C. D.; Whitesides, G. M. Comparison of Organic Monolayers on Polycrystalline Gold Spontaneously Assembled from Solutions Containing Dialkyl Disulfides or Alkanethiols. *Langmuir* **1994**, *10*, 1825−1831.
(98) Lavrich, D. J.; Wetterer, S. M.; Bernasek, S. L.; Scoles, G. Physisorption and Chemisorption of Alkanethiols and Alkyl Sulfides on Au(111). *J. Phys. Chem. B* **1998**, *102*, 3456−3465.
(99) Hakkinen, H. The gold-sulfur interface at the nanoscale. *Nat. Chem.* **2012**, *4*, 443−455.
(100) Zhong, C.-J.; Porter, M. D. Evidence for Carbon-Sulfur Bond Cleavage in Spontaneously Adsorbed Organosulfide-Based Monolayers at Gold. *J. Am. Chem. Soc.* **1994**, *116*, 11616−11617.
(101) Porter, M. D.; Bright, T. B.; Allara, D. L.; Chidsey, C. E. D. Spontaneously organized molecular assemblies. 4. Structural characterization of n-alkyl thiol monolayers on gold by optical ellipsometry, infrared spectroscopy, and electrochemistry. *J. Am. Chem. Soc.* **1987**, *109*, 3559−3568.
(102) Rouhana, L. L.; Moussallem, M. D.; Schlenoff, J. B. Adsorption of Short-Chain Thiols and Disulfides onto Gold under Defined Mass Transport Conditions: Coverage, Kinetics, and Mechanism. *J. Am. Chem. Soc.* **2011**, *133*, 16080−16091.
(103) Hagenhoff, B.; Benninghoven, A.; Spinke, J.; Liley, M.; Knoll, W. Time-of-flight secondary ion mass spectrometry investigations of self-assembled monolayers of organic thiols, sulfides, and disulfides on gold surfaces. *Langmuir* **1993**, *9*, 1622−1624.
(104) Louie, S. M.; Gorham, J. M.; McGivney, E. A.; Liu, J.; Gregory, K. B.; Hackley, V. A. Photochemical transformations of thiolated polyethylene glycol coatings on gold nanoparticles. *Environ. Sci.: Nano* **2016**, *3*, 1090−1102.
(105) Bucher, G.; Lu, C. Y.; Sander, W. The photochemistry of lipoic acid: Photoionization and observation of a triplet excited state of a disulfide. *ChemPhysChem* **2005**, *6*, 2607−2618.
(106) Brown, P. R.; Edwards, J. O. Effect of solvent on the photolysis of. alpha.-lipoic acid. *J. Org. Chem.* **1969**, *34*, 3131−3135.
(107) Brown, P. R.; Edwards, J. O. Use of Thin-Layer Chromatography in Following Product Formation in Photolysis of Alpha-Lipoic Acid. *J. Chromatogr.* **1969**, *43*, 515.
(108) Barltrop, J. A.; Hayes, P. M.; Calvin, M. The Chemistry of 1,2-Dithiolane (Trimethylene Disulfide) as a Model for the Primary Quantum Conversion Act in Photosynthesis. *J. Am. Chem. Soc.* **1954**, *76*, 4348−4367.
(109) Montague, M.; Ducker, R. E.; Chong, K. S. L.; Manning, R. J.; Rutten, F. J. M.; Davies, M. C.; Leggett, G. J. Fabrication of Biomolecular Nanostructures by Scanning Near-Field Photolithography of Oligo(ethylene glycol)-Terminated Self-Assembled Monolayers. *Langmuir* **2007**, *23*, 7328−7337.

https://dx.doi.org/10.1021/acs.chemmater.0c02482
Chem. Mater. 2020, 32, 7469−7483